




A microRNA-129-5p/Rbfox crosstalk coordinates homeostatic downscaling of excitatory synapses

Marek Rajman¹ , Franziska Metge^{2,†}, Roberto Fiore¹, Sharof Khudayberdiev¹, Ayla Aksoy-Aksel^{1,‡}, Silvia Bicker¹ , Cristina Ruedell Reschke³, Rana Raouf³, Gary P Brennan³, Norman Delanty⁴, Michael A Farrell⁴, Donncha F O'Brien⁴, Sebastian Bauer^{5,6}, Braxton Norwood^{5,6}, Morten T Venø⁷, Marcus Krüger^{8,9,10}, Thomas Braun¹¹, Jørgen Kjems⁷, Felix Rosenow^{5,6}, David C Henshall³, Christoph Dieterich² & Gerhard Schratt^{1,*} 

Abstract

Synaptic downscaling is a homeostatic mechanism that allows neurons to reduce firing rates during chronically elevated network activity. Although synaptic downscaling is important in neural circuit development and epilepsy, the underlying mechanisms are poorly described. We performed small RNA profiling in picrotoxin (PTX)-treated hippocampal neurons, a model of synaptic downscaling. Thereby, we identified eight microRNAs (miRNAs) that were increased in response to PTX, including miR-129-5p, whose inhibition blocked synaptic downscaling *in vitro* and reduced epileptic seizure severity *in vivo*. Using transcriptome, proteome, and bioinformatic analysis, we identified the calcium pump *Atp2b4* and doublecortin (*Dcx*) as miR-129-5p targets. Restoring *Atp2b4* and *Dcx* expression was sufficient to prevent synaptic downscaling in PTX-treated neurons. Furthermore, we characterized a functional crosstalk between miR-129-5p and the RNA-binding protein (RBP) *Rbfox1*. In the absence of PTX, *Rbfox1* promoted the expression of *Atp2b4* and *Dcx*. Upon PTX treatment, *Rbfox1* expression was downregulated by miR-129-5p, thereby allowing the repression of *Atp2b4* and *Dcx*. We therefore identified a novel activity-dependent miRNA/RBP crosstalk during synaptic scaling, with potential implications for neural network homeostasis and epileptogenesis.

Keywords epilepsy; homeostatic plasticity; microRNA; RNA-binding protein; synaptic scaling

Subject Categories Neuroscience; RNA Biology

DOI 10.15252/embj.201695748 | Received 16 September 2016 | Revised 5 April 2017 | Accepted 7 April 2017 | Published online 9 May 2017

The EMBO Journal (2017) 36: 1770–1787

Introduction

Neurons possess a sophisticated repertoire of cellular mechanisms that help to maintain homeostasis in response to changes in network activity (e.g., those encountered during circuit development or upon traumatic brain injuries) that would otherwise compromise neuronal function and health. These mechanisms operate either at the level of the network (e.g., excitatory/inhibitory balance) or the neuron (intrinsic excitability/synaptic scaling). The uniform downscaling of excitatory synapses in response to chronic increases in network activity has gained significant attention due to its potential function in reducing neuronal firing rates in epilepsy (Siddoway *et al*, 2014; Swann & Rho, 2014) and its engagement during the activity-dependent development of the visual system (Desai *et al*, 2002; Gao *et al*, 2010). Very recently, downscaling of excitatory synapses was also observed during sleep, suggesting an involvement in memory consolidation (Diering *et al*, 2017).

Despite its clinical and physiological significance, studies investigating the molecular mechanisms of synaptic downscaling are only just emerging. Many studies have focused on the role of activity-dependent mRNA transcription of immediate early genes (e.g., *Plk2*, *Homer1a*, *Arc*, *Narp*), transcriptional repression

1 Biochemisch-Pharmakologisches Centrum, Institut für Physiologische Chemie, Philipps-Universität Marburg, Marburg, Germany

2 Section of Bioinformatics and Systems Cardiology, Klaus Tschira Institute for Integrative Computational Cardiology, Department of Internal Medicine III, German Center for Cardiovascular Research (DZHK), University Hospital Heidelberg, Heidelberg, Germany

3 Physiology & Medical Physics Department, Royal College of Surgeons in Ireland, Dublin, Ireland

4 Beaumont Hospital, Dublin, Ireland

5 Epilepsiezentrum Frankfurt Rhein-Main, Neurozentrum, Goethe-Universität Frankfurt, Frankfurt, Germany

6 Epilepsiezentrum Hessen – Marburg, Philipps-Universität Marburg, Marburg, Germany

7 Department of Molecular Biology and Genetics and Interdisciplinary Nanoscience Center, Aarhus University, Aarhus, Denmark

8 Institute for Genetics, University of Cologne, Cologne, Germany

9 Cologne Excellence Cluster on Cellular Stress Responses in Aging-Associated Diseases (CECAD), University of Cologne, Cologne, Germany

10 Center for Molecular Medicine (CMMC), University of Cologne, Cologne, Germany

11 Max Planck Institute for Heart and Lung Research, Bad Nauheim, Germany

*Corresponding author. Tel: +49 6421 2865020; E-mail: schratt@staff.uni-marburg.de

†Present address: Max Planck Institute for Biology of Ageing, Cologne, Germany

‡Present address: Hertie Institute for Clinical Brain Research & Centre for Integrative Neuroscience, Tübingen, Germany

mediated by MeCP2 and proteasome-dependent protein degradation [e.g., SPAR, GKAP, SHANK, GluA1/2; reviewed in Siddoway *et al* (2014)]. In contrast to transcriptional studies, a potential contribution of mechanisms regulating *de novo* protein synthesis at the post-transcriptional level, such as mRNA translation and/or stability, to synaptic downscaling has not been systematically addressed.

The 3' untranslated regions (UTRs) of mRNAs are major hubs for the regulation of mRNA translation/stability. 3'UTR-dependent gene regulation appears to be particularly prevalent in the brain. For example, recent bioinformatic studies described increased 3'UTR length of brain-enriched transcripts (Miura *et al*, 2013) and mRNAs encoding for presynaptic proteins (Paschou *et al*, 2012). Two families of regulatory molecules, sequence-specific RNA-binding proteins (RBPs) and microRNAs (miRNAs), are the focus of studies that address the mechanisms of 3'UTR-dependent gene regulation. When bound to 3'UTRs, RBPs can have both negative (e.g., FMRP; Li *et al*, 2001) and positive effects (e.g., Hu proteins, Rbfox1/3; Colombrita *et al*, 2013; Lee *et al*, 2016) on mRNA translation and stability. MiRNAs are an extensive family of small non-coding RNAs that repress protein synthesis when bound to their targets (Bartel, 2009). In mature neurons, miRNAs have been implicated in the local control of dendritic protein synthesis and synaptic plasticity (Schratt, 2009). Recently, important roles have been attributed to a few miRNAs in homeostatic synaptic plasticity. miR-92a (Letellier *et al*, 2014) and miR-124 (Hou *et al*, 2015) are involved in synaptic upscaling in response to chronic activity blockade. miR-485 regulates synaptic downscaling by a presynaptic mechanism (Cohen *et al*, 2011). Until now, only one miRNA (miR-134-5p) was shown to regulate synaptic downscaling at postsynaptic sites (Fiore *et al*, 2014). Functional crosstalk between miRNAs and RBPs on the same 3'UTR has been reported in non-neuronal cells (Kedde & Agami, 2008).

In the current study, we present the first comprehensive analysis of miRNA, mRNA, and protein expression in a cellular model of synaptic downscaling. We identify a novel miRNA-RBP crosstalk, consisting of miR-129-5p and Rbfox proteins, that coordinates the expression of important synaptic proteins during downscaling. We further show that this pathway is deregulated in epilepsy, suggesting an involvement in neural network homeostasis. Together, our results indicate a more widespread role of post-transcriptional regulatory mechanisms involving miRNAs and RBPs in homeostatic plasticity than previously anticipated.

Results

A specific set of miRNAs is upregulated during synaptic downscaling *in vitro*

We hypothesized that miRNAs whose expression is regulated by a long-term increase in network activity might represent strong candidates for functionally important molecules in synaptic downscaling. We used mature primary rat hippocampal neurons cultured for 20 days *in vitro* (20 DIV) as a cellular model of synaptic downscaling. In these cells, long-term treatment (48 h) with the GABA-A receptor blocker picrotoxin (PTX) induces elevated network activity followed by synaptic downscaling, as previously shown (Shepherd

et al, 2006; Iyata *et al*, 2008). We could validate efficient synaptic downscaling by showing a PTX-mediated downregulation of surface expression of the AMPA-type glutamate receptor (AMPA-R) GluA1 in these neurons (Fig 1A; Evers *et al*, 2010). To systematically characterize changes in miRNA expression during synaptic downscaling, we performed comparative small RNA sequencing using this PTX model. We identified a total of eight different miRNA species encoded by four different genomic miRNA loci that were differentially regulated (FDR < 0.05) in PTX- compared to vehicle-treated neurons (Fig 1B; Table EV1). Intriguingly, all of these miRNAs were upregulated by PTX, consistent with a repressive function during PTX-induced downscaling. Four miRNAs (miR-212-3p/5p, miR-132-3p/5p) are encoded by the miR-132–212 cluster, which was previously implicated in activity-dependent synapse development and remodeling (Wanet *et al*, 2012). Two miRNAs (miR-495, miR-543-3p) are part of the large imprinted miR379–410 cluster, members of which have been implicated in neuronal morphogenesis (Schratt *et al*, 2006; Fiore *et al*, 2009) and homeostatic synaptic scaling (Fiore *et al*, 2014). The remaining two miRNAs have not been studied in the context of synapse development and homeostasis. The most PTX-responsive miRNA, miR-155-5p, displays only very weak expression in nerve cells and was mostly studied in the immune system (Su *et al*, 2016). In contrast, miR-129-5p is abundantly expressed in the developing retina (Decembrini *et al*, 2009) and in hippocampal neurons, where it was shown to control neuronal excitability by regulating the expression of the potassium channel Kv1.1 (Sosanya *et al*, 2013). We therefore decided to investigate a potential involvement of miR-129-5p in the regulation of synaptic downscaling.

miR-129-5p is required for homeostatic synaptic downscaling in the cellular PTX model

Using qPCR, we validated that 48-h PTX treatment of hippocampal neurons induces mature miR-129-5p expression in a similar manner to the known activity-regulated miR-132-3p (Remenyi *et al*, 2010; Fig 1C). We tested whether miR-129-5p is required for synaptic downscaling in hippocampal neurons. To address this, we applied specific antisense oligonucleotide inhibitors of miR-129-5p (anti-miR-129) in vehicle- and PTX-treated neurons and monitored dendritic spine size by confocal fluorescence microscopy (Fig 2A). Dendritic spine size is a correlate of postsynaptic strength and uniformly reduced in 48-h PTX-treated neurons (Fiore *et al*, 2014). The efficacy and specificity of the anti-miRs was validated in miR-129-5p sensor assays (Appendix Fig S1A). We found that inhibition of miR-129-5p completely abolished PTX-mediated spine size reduction compared to cells transfected with GFP only or a control inhibitor (anti-miR Control; Fig 2A), demonstrating that miR-129-5p is required for PTX-dependent downscaling of dendritic spine size. Spine size was already reduced in anti-miR-129-5p-transfected neurons in the absence of PTX, suggesting that miR-129-5p has an additional, activity-independent spine growth promoting effect (Appendix Fig S1B). In addition, overexpression of miR-129-5p in the absence of PTX decreased spine size, indicating that miR-129-5p is sufficient to induce spine shrinkage (Appendix Fig S1C). To examine effects on synaptic strength more directly, we performed patch-clamp electrophysiological recordings of miniature excitatory postsynaptic currents (mEPSCs). We used the competitive GABA-A

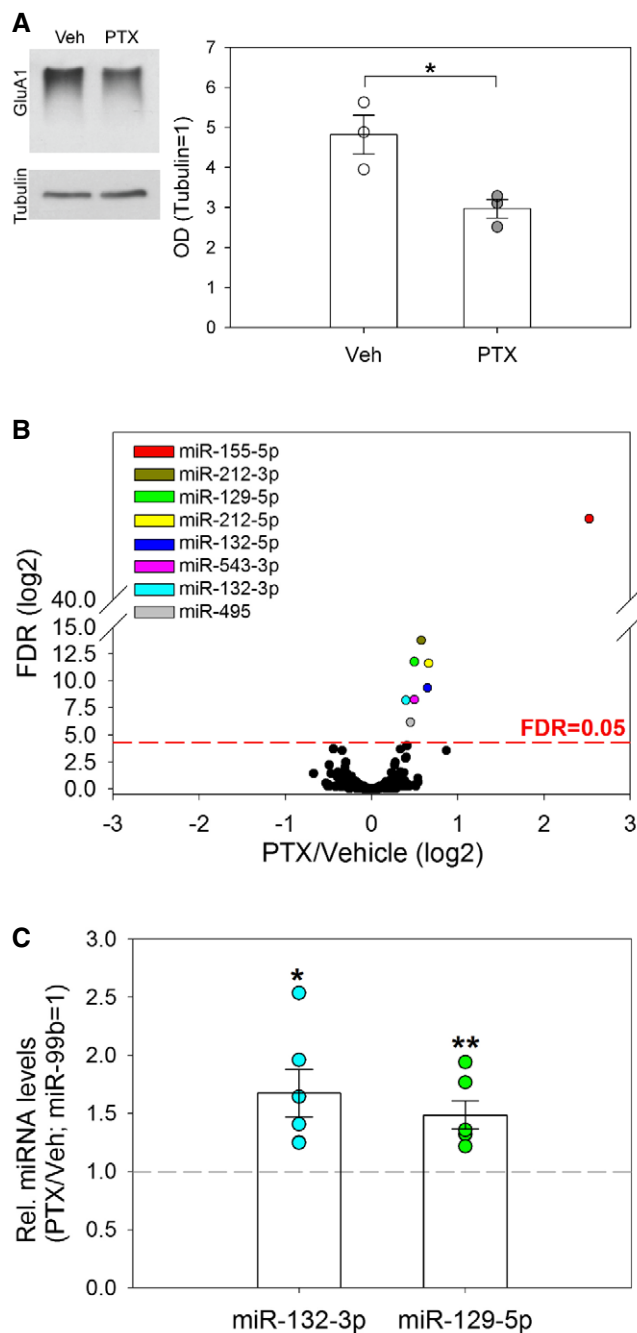


Figure 1. A specific set of miRNAs is upregulated during synaptic downscaling *in vitro*.

A Western blot analysis of surface GluA1 expression after cross-linking in lysates from vehicle (Veh)- or prototoxin (PTX, 48 h)-treated hippocampal neurons. Left: Representative Western blot. Tubulin was used as a loading control. Right: Quantification of Western blot data from three independent experiments. Dot-blot presentation with mean optical band density (OD) normalized to tubulin \pm s.e.m. (independent two-sample *t*-test, two-tailed, homoscedastic variance; **P* = 0.026).

B Average changes in miRNA levels (PTX/Veh; log₂) as determined by small RNA-seq (*n* = 3,442 miRNAs; correction for multiple comparisons by FDR, *P* < 0.05). miRNAs significantly upregulated by PTX are highlighted.

C TaqMan qPCR analysis of miR-129-5p and miR-132-3p in PTX- and vehicle-treated hippocampal neurons. Dot-plot presentation with mean relative miRNA levels (PTX/Veh) normalized to miR-99b \pm s.e.m. (*n* = 6; independent one-sample *t*-test, two-tailed, heteroscedastic variance; **P* = 0.022, ***P* = 0.010).

Source data are available online for this figure.

miR-129-5p is involved in the regulation of epileptic seizures *in vivo*

A chronic overexcitation of neural networks is observed in the epileptic brain during seizure activity. Furthermore, it was hypothesized that homeostatic plasticity mechanisms are actively engaged in the epileptic brain (Swann & Rho, 2014). We therefore decided to study a potential involvement of miR-129-5p in the regulation of epileptic seizures *in vivo*. First, we investigated miR-129-5p expression in rats in which mesial TLE with hippocampal sclerosis was induced by 8 h of perforant pathway stimulation (PPS; Norwood *et al*, 2011). This toxin-free animal model reliably replicates essential characteristics of acquired human TLE. We found that Ago2-associated miR-129-5p was significantly elevated at 1, 24, and 72 h after 8-h PPS (Fig 3A). Thereafter (8 h + 10 days, 8 h + 16 days), miR-129-5p levels returned close to baseline. Intriguingly, Ago2-associated miR-129-5p levels were again induced 30-days post-spontaneous seizure, suggesting that network hyperactivity associated with seizures could increase miR-129-5p Ago2 association. Ago2 association of miR-129-5p in the epileptic brain was specific, since expression of the corresponding miRNA* sequences (miR-129-1-3p and miR-129-2-3p) was not significantly altered at any time point after PPS (Appendix Fig S2A and B). We next asked whether induction of miR-129-5p was functionally involved in pathological brain activity *in vivo*. Therefore, we pretreated mice with anti-miR-129 or PBS (intracerebroventricular injection) 24 h before inducing status epilepticus by intra-amygdalar injection of kainic acid (KA). We used the KA model for functional testing, since it is less time- and resource-consuming and well established for the use of anti-miRs (Jimenez-Mateos *et al*, 2011, 2012, 2015; McKiernan *et al*, 2012). We validated that miR-129-5p was robustly induced by KA injection (Appendix Fig S2C). In control experiments, we found that multiple EEG parameters were not significantly different between animals injected with PBS or a scrambled oligonucleotide (anti-miR control; Appendix Fig S3), indicating that PBS-injected animals represent adequate controls. Compared to PBS pretreated mice, anti-miR-129-5p pretreatment strongly reduced seizure severity in KA-injected mice (Fig 3B–D; Appendix Fig S4A) and the total time mice spent in seizures (Fig 3E), as judged by EEG. Furthermore, anti-miR-129-5p pretreatment strongly suppressed KA-induced cell death in different hippocampal subfields, as judged by Fluoro-Jade B (FJB) staining (Fig 3F and G;

receptor blocker bicuculline (Bic) in these experiments, since electrophysiological recordings were more stable with Bic compared to PTX. Importantly, results from different sets of experiments (Appendix Fig S1D–F; Table EV2) demonstrate that the effects of Bic and PTX on synaptic gene expression and spine morphogenesis were overall comparable. Anti-miR-129-5p strongly attenuated the Bic-mediated reduction in mean mEPSC amplitude compared to anti-miR control (Fig 2B). Thus, miR-129-5p activity is required for an efficient morphological and physiological downscaling of excitatory synapses in hippocampal neurons in response to chronically elevated network activity.

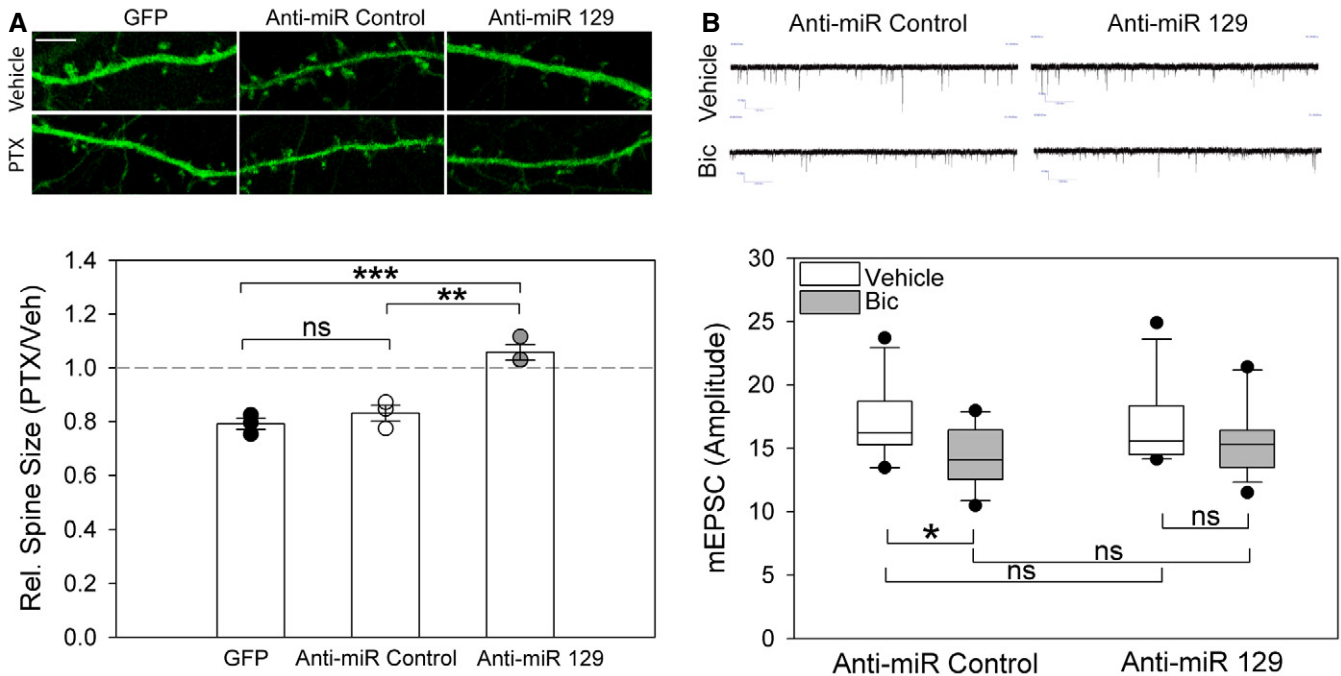


Figure 2. miR-129-5p is required for synaptic downscaling *in vitro*.

A Upper panel: Representative confocal microscopy images of dendritic segments from PTX- or vehicle (Veh)-treated hippocampal neurons transfected with indicated anti-miRs (scale bar = 5 μ m). Bottom panel: Quantification of dendritic spine size from three independent experiments. Dot-plot presentation with mean relative spine size (Ptx/Veh) \pm s.e.m. ($n = 3$; 8 neurons, \sim 200 spines/neuron per experimental condition; one-way ANOVA; $F(2,6) = 29.31$, $P = 0.001$; groups were compared by Bonferroni *post hoc* test; $**P = 0.0030$, $***P = 0.001$, ns: not significant).

B Upper panel: Representative traces of mEPSC recordings from bicuculline (Bic)- or vehicle-treated neurons transfected with indicated anti-miRs. Bottom panel: Quantification of mEPSC amplitudes from multiple neurons, data are presented as box plots (anti-miR Control Veh/Bic $n = 13/12$; anti-miR-129 Veh/Bic $n = 14/13$; GLM model; activity $P = 0.015$; estimated means of specific experimental conditions were compared by pairwise comparison in SPSS; anti-miR Control Veh vs. Bic $*P = 0.023$; anti-miR-129-5p Veh vs. Bic $P = 0.242$; Veh anti-miR Control vs. anti-miR-129-5p $P = 0.827$; Bic anti-miR Control vs. anti-miR-129-5p $P = 0.307$; ns: not significant). The boundary of the box closest to zero indicates the 25th percentile, a line within the box marks the median, and the boundary of the box farthest from zero indicates the 75th percentile. Error bars above and below the box indicate the 90th and 10th percentiles.

Appendix Fig S4B–D). Forty minutes after KA-induced status epilepticus, all mice were injected with lorazepam to reduce mortality and morbidity. A similar seizure-suppressive effect of anti-miR-129-5p was also observed after lorazepam administration (Appendix Fig S4E–H). Successful inhibition of miR-129-5p *in vivo* was confirmed

by qPCR (Appendix Fig S4I). Anti-miR-129-5p did not alter EEG parameters during baseline measurement prior to KA injection (Appendix Fig S4J–L). Our data suggest that miR-129-5p induction in the hippocampus *in vivo* promotes seizure activity and associated neurodegeneration. Finally, we analyzed brain samples from human

Figure 3. miR-129-5p is involved in the regulation of epileptic seizures *in vivo*.

A Small RNA-seq analysis of Ago2-associated miR-129-5p from the dentate gyrus of rats at indicated times after perforant path stimulation (PPS) or after the occurrence of the first seizure (post-spontaneous seizure). Data are presented as fold (\log_2) induction over control-treated rats in a dot plot with mean \pm s.e.m. (one-way ANOVA, correction for multiple comparisons by Benjamini–Hochberg FDR, $P = 0.005$; $n = 3$ per experimental condition, $*P < 0.05$, $***P < 0.01$). Average levels of Ago2-associated miR-129-5p in control group were set to 0 (\log_2).

B Representative heatmap showing frequency (Hz) and amplitude (μ V) of EEG recordings over time (in minutes) for a control (PBS)- and anti-miR-129-5p-injected mice, followed by the respective EEG traces immediately below.

C–E Graphs show EEG total power (C), amplitude (D), depicting % of increase from each animal's own baseline data, and time spent in seizures (E) during 40 min of observation after KA-induced status epilepticus in mice pretreated (24 h) with PBS or anti-miR-129-5p. Dot-plot presentation with mean \pm s.e.m. ($n = 4$ –5 mice per group; independent two-sample *t*-test, two-tailed, homoscedastic variance; total power $*P = 0.0421$, amplitude $*P = 0.041$, time in seizures $**P = 0.0012$).

F Representative photomicrographs from Fluoro-Jade B (FJB) stainings of the mouse dorsal hippocampus 24 h after status epilepticus. Mice were injected with PBS or anti-miR-129-5p 24 h before KA administration. Scale bar = 100 μ m.

G Quantification of FJB-positive cells from multiple slices performed in (F). Dot-plot presentation with mean cell count \pm s.e.m. ($n = 4$ –5 mice per group; independent two-sample *t*-test, two-tailed, homoscedastic variance; $**P = 0.009$).

H TaqMan qPCR analysis of miR-129-5p levels in the hippocampus of human temporal lobe epilepsy (TLE) patients displaying hippocampal sclerosis (HS) ($n = 6$) or healthy controls ($n = 10$). Dot-plot presentation with mean relative miR-129-5p levels (\log_2) \pm s.e.m. (independent two-sample *t*-test, two-tailed, homoscedastic variance; $**P = 0.004$).

temporal lobe epilepsy (TLE) patients. Using qPCR, we found that miR-129-5p was significantly higher expressed in the hippocampus of TLE patients displaying hippocampal sclerosis (HS) compared to age-matched healthy controls (Fig 3H, Table EV3). MiR-129-5p levels were also elevated in TLE patients without confirmed hippocampal sclerosis, although this did not reach statistical significance (Appendix Fig S5A). These results suggest that miR-129-5p dysregulation is conserved between the rodent and human epileptic brain.

Systematic miRNA target identification using a combination of RNA-seq and quantitative proteomics

To obtain further insight into the mechanism of miR-129-5p-regulated synaptic downscaling, we were interested in identifying miR-129-5p target mRNAs. Since we observed that miR-129-5p expression was upregulated by PTX, we expected that miR-129-5p targets should be overrepresented in PTX-downregulated mRNAs. miRNA target site

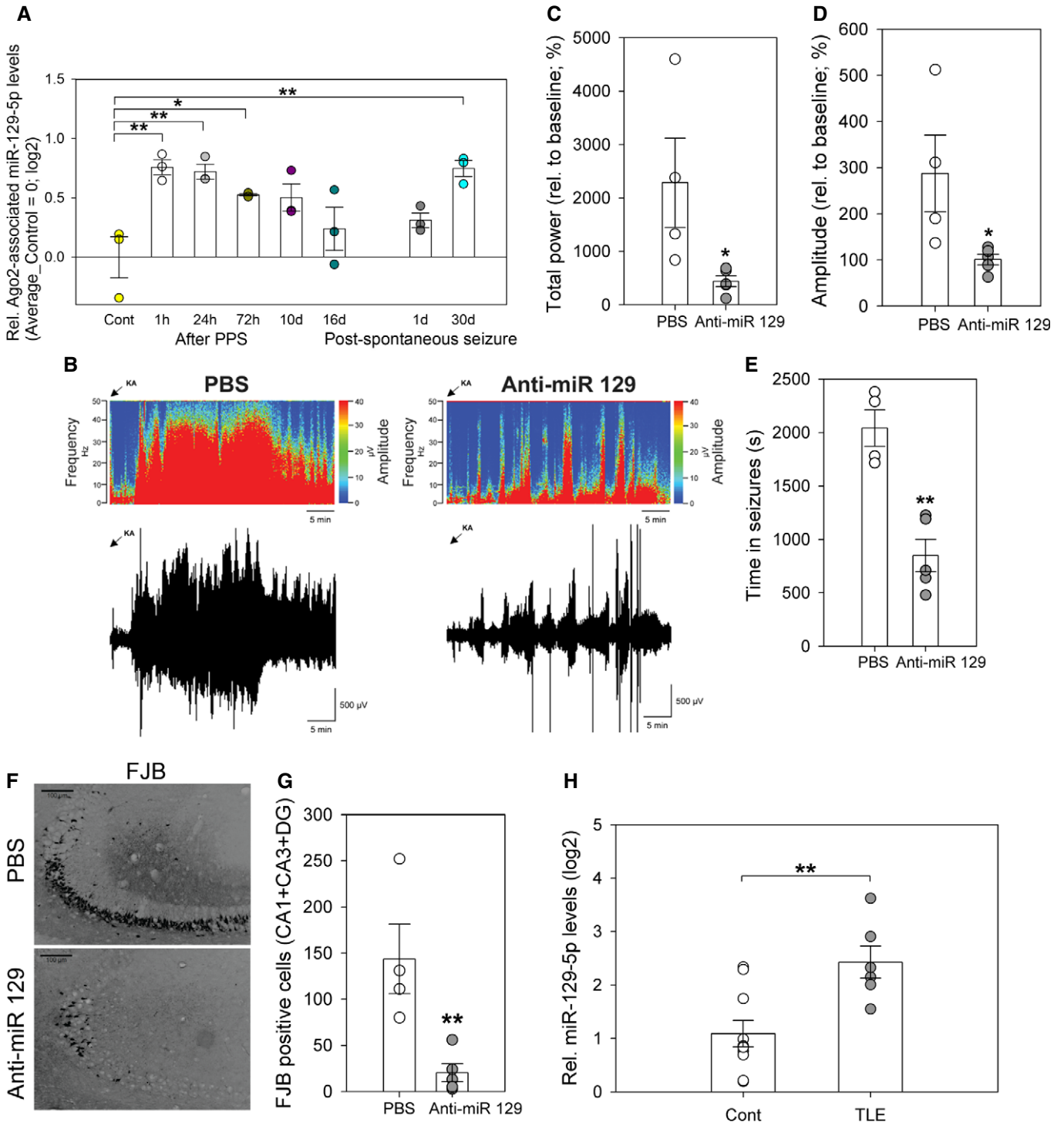


Figure 3.

Figure 4. Systematic miRNA target identification using a combination of RNA-seq and quantitative proteomics.

- A Average changes in mRNA levels (PTX/Veh; log₂) as determined by polyA RNA-seq ($n = 3$; q -values represent FDR-corrected P -values; $q < 0.05$); 495 genes were significantly upregulated and 462 genes were significantly downregulated upon PTX treatment.
- B GO term analysis for 957 genes with differentially regulated mRNA levels upon 48-h PTX treatment (Fig 4A). The color of the central column elements represents GO term enrichment in the analyzed dataset. Numbers in the central column represent total number of genes associated with the specific GO term. Percentage in the downregulated or upregulated group stands for identified number of genes associated with specific GO term in the experimental dataset.
- C qPCR analysis of indicated candidate genes using polyA RNA from PTX (48 h)- or vehicle-treated hippocampal neurons. Dot-plot presentation with mean relative RNA levels (PTX/Veh (log₂)) \pm s.e.m. ($n = 4$ independent experiments; independent one-sample t -test, two-tailed, heteroscedastic variance; *Atp2b4* * $P = 0.033$, *Camk2a* * $P = 0.023$, *Dcx* $P = 0.062$, *Camk2b* $P = 0.450$; ns: not significant).
- D Left panel: Timeline of pSILAC experiment in primary hippocampal neurons cultured for indicated number of days *in vitro* (DIV). Right panel: Average changes in new protein synthesis (PTX/Veh; log₂) plotted vs. P -value (log₂) ($n = 3$; 1,225 proteins; independent one-sample t -test, two-tailed, heteroscedastic variance). Proteins with $P < 0.05$ were considered as differentially synthesized (total of 182 proteins, 97 \downarrow , 85 \uparrow).
- E Western blot analysis of *Atp2b4*, *Camk2a*, *Syn1*, *Dcx*, *GluA1*, *Ago2*, and 4E-BP1 expression in lysates from vehicle (Veh)- and PTX (48 h)-treated hippocampal neurons. Left: Representative Western blot. Tubulin was used as a loading control. Right: Quantification of four independent experiments except *Ago2* ($n = 3$) and *Syn1* ($n = 5$). Dot-plot presentation with mean relative protein levels (PTX/Veh) \pm s.e.m. (independent one-sample t -test, two-tailed, heteroscedastic variance; *Atp2b4* * $P = 0.012$, *Camk2a* ** $P = 0.005$, *Dcx* * $P = 0.026$, 4E-BP1 $P = 0.09$, *Syn1* *** $P = 0.005$, *Ago2* *** $P = 0.005$, *GluA1* * $P = 0.03$; ns: not significant).
- F Overlap of genes displaying differential mRNA levels (panel A) and new protein synthesis (panel D). mRNA fold changes (PTX/Veh; log₂) are plotted vs. fold changes in new protein synthesis (PTX/Veh; log₂). Pearson's correlation was used to compare changes at the mRNA and protein synthesis level.
- G Box plot representation of the 3'UTR length of genes that are significantly regulated by PTX based on pSILAC (left; panel D) or RNA-seq (right; panel A) (Mann–Whitney U -test; *** $P < 0.001$).
- H Abundance of binding sites (8mer-1a and 7mer-m8 seeds) for differentially regulated miRNAs (Fig 1B) in 3'UTRs of genes that are significantly regulated by PTX based on pSILAC (panel D) or RNA-seq (panel A) according to TargetScan-Human version 6.2. D: decreased; I: increased. Seeds were classified as poorly conserved (≤ 3 species), conserved (4–9 species), or highly conserved (≥ 10 species). Bar graphs represent total number of miRNA binding sites per group. Numbers above bars represent the ratio of total miRNA binding sites between decreased and increased genes.

Source data are available online for this figure.

prediction in PTX-downregulated mRNAs should then allow to enrich for direct miR-129-5p targets. Comparative mRNA profiling from PTX- and vehicle-treated neurons using polyA RNA sequencing (Fig 4A; Table EV4) allowed us to monitor the expression of RNAs derived from roughly 9,000 genes. Of those, 957 were differentially expressed (q -value < 0.05) between 48-h PTX- and vehicle-treated neurons based on three biological replicates. Gene ontology (GO) term analysis suggests that PTX-decreased genes, in contrast to increased genes, are mainly associated with synaptic functions (Fig 4B), for example, glutamate receptor signaling, calcium-mediated signaling, and synaptic plasticity. Accordingly, known regulators of synaptic scaling were mostly found among the PTX-downregulated genes (e.g., *GluA1*, *Ppp3ca*, *Akap5*, *Camk2a*; Groth *et al*, 2011; Diering *et al*, 2014; Kim & Ziff, 2014). We could validate a PTX-dependent reduction in mRNA levels for several candidates using qPCR (Fig 4C) and fluorescence *in situ* hybridization (Appendix Fig S5B–D).

Next, we investigated whether changes observed at the mRNA level translated into corresponding alterations in *de novo* protein synthesis. Changes in *de novo* protein synthesis during PTX treatment were quantified by pulsed stable isotope labeling of amino acids in culture (pSILAC) (Selbach *et al*, 2008) followed by mass spectrometry. Briefly, neurons were incubated with Arg6/LysD4 starting at 15 DIV, PTX was applied at 18 DIV, and proteins were extracted at 20 DIV and analyzed by mass spectrometry (Fig 4D; please refer to the Appendix Results, including Appendix Fig S5E–I and Tables EV5 and EV6, for a more detailed characterization of pSILAC experiments). In total, we were able to reproducibly detect 1225 proteins in three independent neuron preparations (Fig 4D). Of those, expression of 182 proteins was significantly ($P < 0.05$) different between PTX- and vehicle-treated cultures (97 decreased, 85 increased; Table EV7). Similar to the analysis of differentially expressed mRNAs, GO terms for downregulated proteins identified by pSILAC were specifically enriched for synaptic functions (Appendix Fig S5J). We validated PTX regulation for five

significantly downregulated (*Atp2b4*, *Camk2a*, *Syn1*, *Dcx*, *GluA1*) and one upregulated protein (*Ago2*) using Western blot (Fig 4E). *Dcx* protein was included in the validation experiments since it represented the top downregulated protein in two out of three pSILAC replicates. Importantly, changes in *de novo* protein synthesis and mRNA levels were significantly correlated for the set of PTX-repressed, but not PTX-induced genes (Fig 4F). This result suggests that a large fraction of PTX-downregulated genes are coordinately regulated at the mRNA and protein level.

Interestingly, 3'UTRs corresponding to PTX-decreased genes were on average more than twice as long as 3'UTRs corresponding to PTX-increased genes (Fig 4G; New Protein—differentially expressed proteins; 3'UTR length calculated based on RNA-seq data; median: 1.03 kb (decreased) vs. 0.33 kb (increased); mRNA—differentially expressed genes; \downarrow mRNAs median: 1.3 kb vs. \uparrow mRNAs median: 0.7 kb; Tables EV8 and EV9). In contrast, 5'UTRs are in general much shorter, and their length is not significantly different between PTX-regulated genes (Appendix Fig S6A and B New Protein/mRNA). This result suggests an involvement of 3'UTR-dependent post-transcriptional mechanisms in PTX-mediated gene repression. We next determined the frequency of miRNA binding sites in the 3'UTRs corresponding to differentially PTX-regulated proteins and mRNAs using the TargetScan algorithm. We found that binding sites for PTX-upregulated miRNAs were in general more abundant in the 3'UTRs of downregulated compared to upregulated genes (Fig 4H; Tables EV10 and EV11). Importantly, miR-129-5p binding sites were among the most strongly enriched sites in PTX-repressed genes, consistent with an important contribution of miR-129-5p to the regulation of PTX-responsive genes.

***Atp2b4* and *Dcx* are miR-129-5p target genes**

To narrow down on direct targets of miR-129-5p, we intersected the datasets obtained with proteomics, transcriptomics, and miRNA

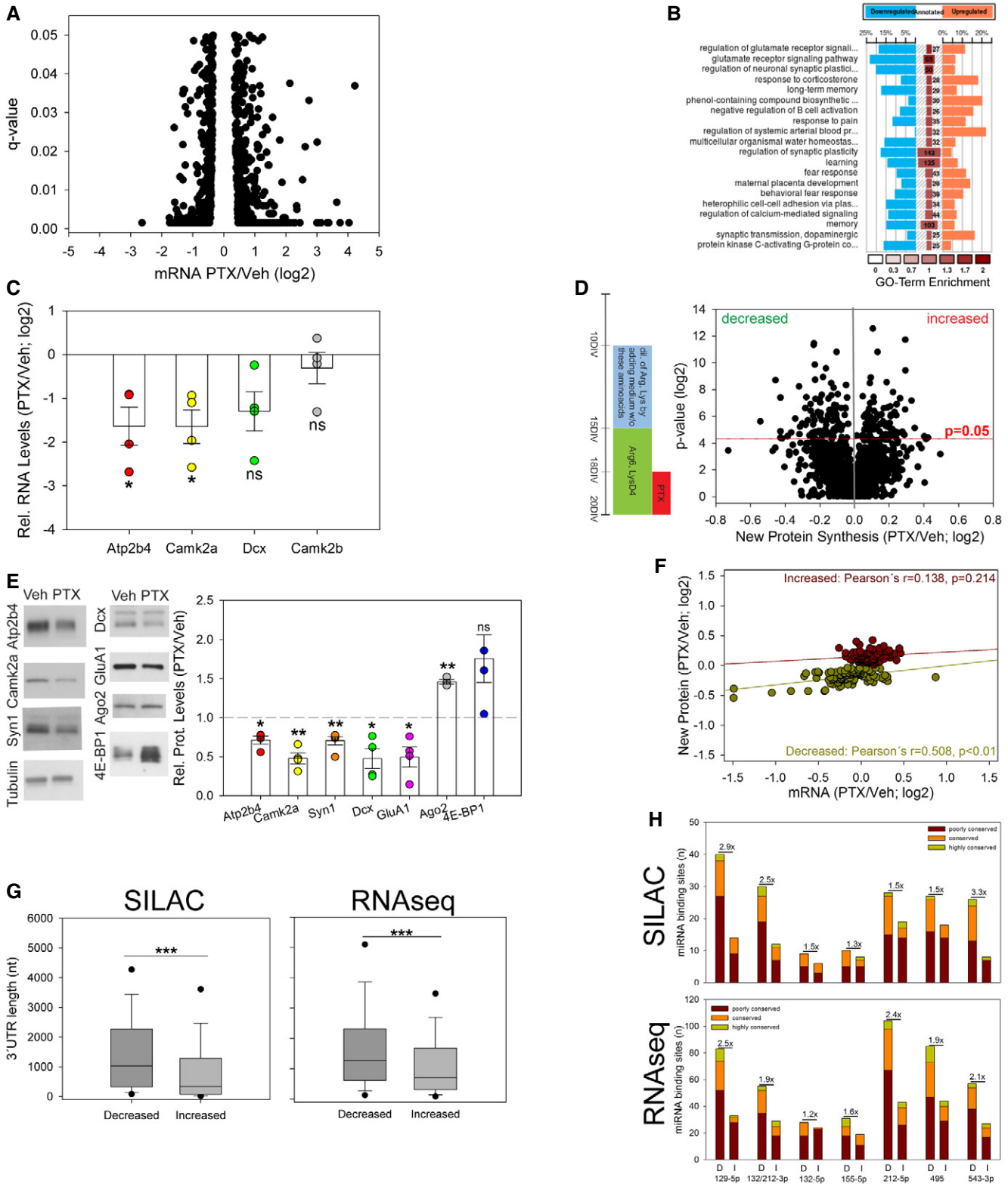


Figure 4.

target prediction. Thereby, we identified six genes that were significantly downregulated by PTX at the mRNA and protein level and contain at least one miR-129-5p binding site (Fig 5A). We focused

on *Atp2b4* and *Dcx*, since both contain one highly conserved miR-129-5p binding site in their 3'UTR (Fig 5B). We further hypothesized that the regulation of these genes could be functionally

Figure 5. *Atp2b4* and *Dcx* are miR-129-5p target genes.

- A List of predicted miR-129-5p targets (TargetScan-Human version 6.2) that were significantly downregulated by PTX in both pSILAC (Fig 4D) and RNA-seq (Fig 4A) experiments.
- B Localization of miR-129-5p binding sites (as predicted in Fig 4H) in the 3'UTRs of *Atp2b4* and *Dcx*. Color code indicates different degree of conservation.
- C Western blot analysis of *Atp2b4*, *Dcx*, and actin protein expression in hippocampal neurons transfected with miR-129-5p or control duplex RNA. Left: Representative Western blot. Tubulin was used as a loading control. Right: Quantification of multiple experiments. Dot-plot presentation with mean relative protein levels (miR-129-5p/control) \pm s.e.m. (*Atp2b4*, *Dcx* $n = 3$; actin $n = 5$; independent one-sample *t*-test, two-tailed, heteroscedastic variance; *Atp2b4* $^*P = 0.0437$, *Dcx* $^*P = 0.0236$, actin $P = 0.4222$; ns: not significant).
- D Luciferase reporter gene assay in miR-129-5p or control duplex RNA-transfected cortical neurons co-transfected with the indicated 3'UTR reporter constructs containing wild-type (wt) or mutated (129mut) miR-129-5p binding sites. Dot-plot presentation with mean relative luciferase activity (miR-129-5p/control) \pm s.e.m. Effect of miR-129-5p was tested by one-sample *t*-test ($n = 4$; two-tailed, heteroscedastic variance; *Atp2b4*-luc wt $^*P = 0.027$, *Atp2b4*-luc 129mut $P = 0.151$, *Dcx*-luc wt $^*P = 0.022$, *Dcx*-luc 129mut $P = 0.082$) or two-sample *t*-test (two-tailed, homoscedastic variance; *Atp2b4* wt vs. 129mut $^{**}P = 0.004$; *Dcx* wt vs. 129mut $P = 0.302$).
- E Luciferase reporter gene assay in vehicle (Veh)- or PTX-treated hippocampal neurons transfected with the *Atp2b4* 3'UTR and *Dcx* 3'UTR reporter construct containing either wt or 129mut binding sites (see panel D). Dot-plot presentation with mean relative luciferase activity (PTX/Veh) \pm s.e.m. pGI4 (PTX/Veh) was set to 1. Effect of PTX was tested by one-sample *t*-test (*Atp2b4*-luc $n = 5$; *Dcx*-luc $n = 4$; two-tailed, heteroscedastic variance; *Atp2b4*-luc wt $^*P = 0.003$, 129mut $P = 0.117$, *Dcx*-luc wt $^*P = 0.004$, 129mut $P = 0.213$) or two-sample *t*-test (two-tailed, homoscedastic variance; *Atp2b4*-luc wt vs. Mut $^{**}P = 0.008$; *Dcx*-luc wt vs. Mut $P = 0.190$, ns: not significant).
- F Western blot analysis of *Atp2b4* and *Dcx* protein expression in PTX- or mock-treated hippocampal neurons that were transfected with the indicated anti-miRs. Left: Representative Western blot. Tubulin was used as a loading control. Right: Quantification of three independent experiments. Dot-plot presentation with mean relative protein levels (PTX/Veh) \pm s.e.m. ($n = 3$; one-way ANOVA; *Atp2b4*: $F(2,6) = 10.323$, $P = 0.011$; groups were compared by Bonferroni *post hoc* test; anti-miR-129-5p vs. anti-miR Cont $^*P = 0.044$; anti-miR-129-5p vs. Empty $^*P = 0.015$; *Dcx*: one-way ANOVA; $F(2,6) = 0.243$; $P = 0.791$).
- G, H Correlation of miR-129-5p and *Atp2b4* (G) or *Dcx* (H) mRNA expression levels in the hippocampus of human TLE patients. Data are presented as rel. RNA or miRNA levels in log₂ scale (*Atp2b4*: $n = 15$, Pearson's $r = -0.706$; $P = 0.003$; *Dcx*: $n = 8$, Pearson's $r = -0.745$; $P = 0.034$).

Source data are available online for this figure.

relevant in synaptic downscaling. *Atp2b4* is an ATP-dependent calcium pump involved in the regulation of calcium homeostasis (Strehler et al, 2007), consistent with the reported central role of calcium-dependent signaling pathways in downscaling (Turrigiano, 2012). *Dcx* is a microtubule-associated protein involved in the regulation of neuronal cell migration and spine morphogenesis (Yoshihara et al, 2014).

We found that transfecting hippocampal neurons with miR-129-5p mimics significantly reduced endogenous protein levels of *Atp2b4* and *Dcx* using Western blotting (Fig 5C). Thus, elevated miR-129-5p levels were sufficient to repress *Atp2b4* and *Dcx* in the absence of PTX. We next investigated whether the observed miR-129-5p-dependent repression of *Atp2b4* and *Dcx* was mediated by the respective 3'UTRs. Transfection of miR-129-5p mimics significantly downregulated the expression of wild-type (wt) *Atp2b4* and *Dcx* 3'UTR luciferase reporters (*Atp2b4*-luc wt, *Dcx*-luc wt; Fig 5D). The repressive effect of miR-129-5p was largely abolished when using an *Atp2b4* luciferase reporter with a mutated miR-129-5p binding site (129 Mut), but only attenuated when using the respective *Dcx*-luc 129 Mut reporter (Fig 5D). To explore the role of the endogenous miR-129-5p in the regulation of *Atp2b4* and *Dcx*, we performed luciferase assays in PTX-treated hippocampal neurons (Fig 5E). Whereas the expression of both wt reporters was significantly decreased by PTX, mutation of the miR-129-5p fully abolished PTX-mediated downregulation of *Atp2b4* (Fig 5E). Similar to miR-129-5p overexpression experiments (Fig 5D), mutation of the miR-129-5p site in *Dcx* only slightly attenuated reporter gene repression by PTX. These results strongly suggest that miR-129-5p regulates *Atp2b4* primarily via the conserved miR-129-5p binding site within its 3'UTR. In contrast, the miR-129-5p site within the *Dcx* 3'UTR only contributes to a minor extent to miR-129-5p-mediated *Dcx* repression. In addition, transfection of anti-miR-129-5p interfered with the PTX-mediated decrease of endogenous *Atp2b4*, but not *Dcx* protein (Fig 5F), consistent with our results from reporter

gene assays. We also found that the expression of miR-129-5p and either *Atp2b4* (Fig 5G) or *Dcx* (Fig 5H) mRNA were inversely correlated in human TLE patients, but not healthy controls (Appendix Fig S6C and D). This finding is consistent with an inhibitory interaction between miR-129-5p and *Atp2b4*/*Dcx* in the human epileptic brain. Taken together, our data strongly suggest that *Atp2b4* and *Dcx* mRNAs are targeted by miR-129-5p during PTX-induced synaptic downscaling. Whereas *Atp2b4* downregulation is strictly miR-129-5p-dependent, the repression of *Dcx* likely involves additional miR-129-5p-independent mechanisms.

Downregulation of miR-129-5p targets *Atp2b4* and *Dcx* is required for synaptic downscaling

We next determined the functional relevance of the downregulation of *Atp2b4* and *Dcx* in synaptic downscaling. Toward this end, we restored *Atp2b4* and *Dcx* expression in PTX-treated hippocampal neurons using transfection of the respective cDNAs. Using confocal microscopy, we observed a significant reduction in spine size upon 48-h PTX treatment in neurons transfected with GFP only or an unrelated control protein (Fig 6A). In contrast, spine size was no longer reduced in PTX-treated neurons transfected with either *Atp2b4* or *Dcx* expression plasmids (Fig 6A). *Atp2b4* or *Dcx* overexpression had no significant effect on spine size in the absence of PTX (Appendix Fig S6E). Thus, downregulation of either *Atp2b4* or *Dcx* is required for the downscaling of spine size upon PTX treatment. Next, we measured mEPSC amplitudes (Fig 6B), focusing on *Atp2b4*-transfected neurons. Consistent with our results from spine size analysis in both PTX- (Fig 6A) and Bic-treated neurons (Appendix Fig S1D), *Atp2b4* overexpression prevented the decrease in mEPSC amplitudes caused by Bic, but had no effect in vehicle-treated neurons (Fig 6B). Taken together, our results demonstrate that downregulation of miR-129-5p targets is critical for morphological (*Atp2b4*, *Dcx*) and functional (*Atp2b4*) synaptic downscaling in hippocampal neurons.

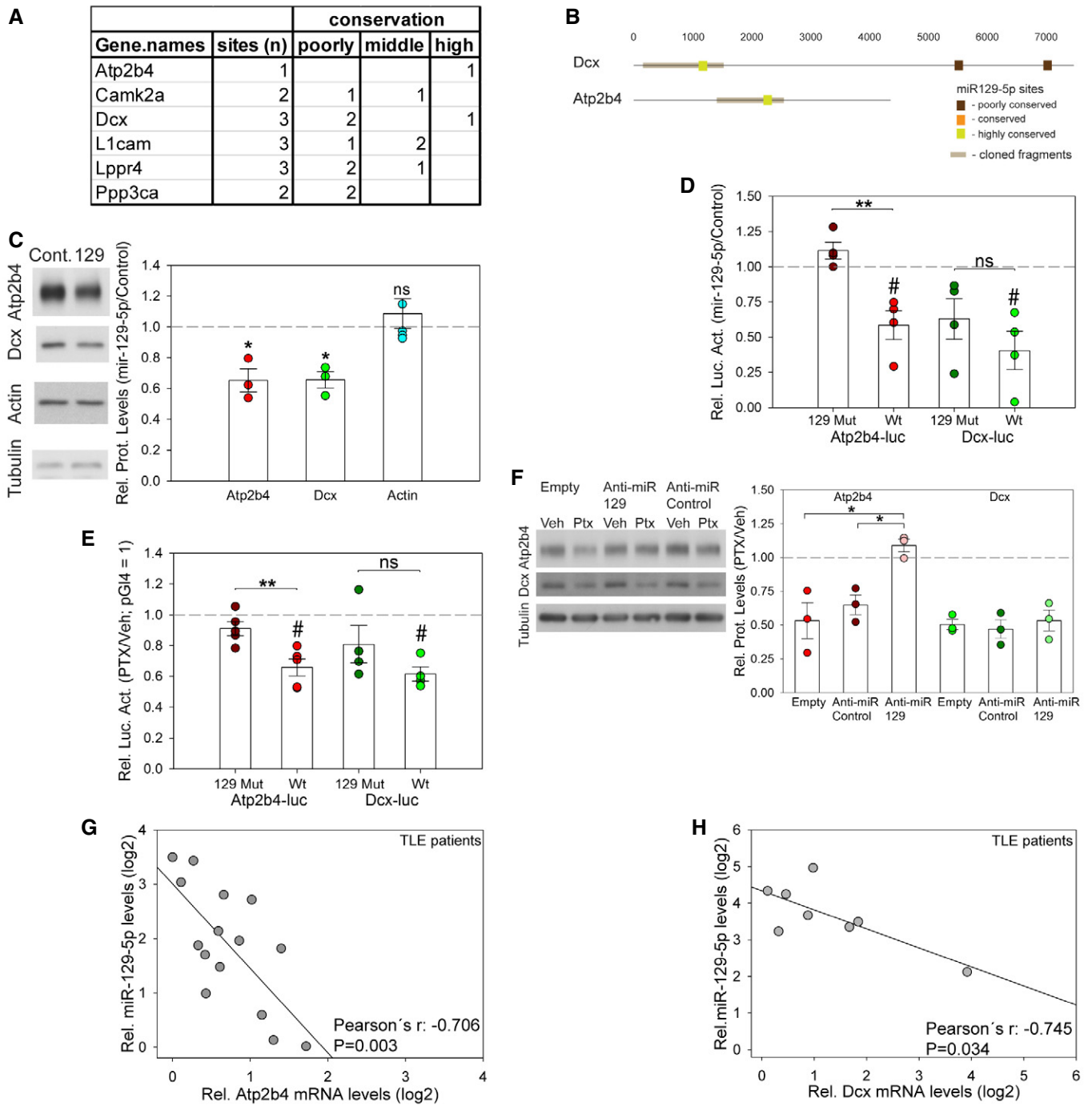


Figure 5.

Rbfox1 is a positive regulator of Dcx and Atp2b4 expression

In addition to miRNAs, RBPs have been shown to regulate post-transcriptional gene expression by binding to conserved sequence elements within the 3'UTR of target mRNAs (Martin & Ephrussi, 2009). To narrow down on functionally important RBPs, we re-analyzed CLIP experiments for nine different RBPs (Chi et al, 2009; Polymenidou et al, 2011; Charizanis et al, 2012; Ince-Dunn et al, 2012; Ishigaki et al, 2012; Licatalosi et al, 2012; Wang et al, 2012;

Lovci et al, 2013) that were performed in mouse brain. Thereby, we found that binding sites for Fus, Mbnl1/2, and Rbfox1/2/3 were most significantly ($P < 0.001$) overrepresented in the 3'UTR of PTX-decreased genes compared to PTX-increased genes (Fig 7A). Of those, Rbfox family members (Rbfox 1–3) were of particular interest, since Rbfox1/3 were recently shown to promote mRNA stability and translation of synaptic genes, including *Camk2a* (Lee et al, 2016).

The Rbfox consensus binding motif ((U)GCAUG) was strongly overrepresented in 3'UTRs corresponding to PTX-decreased genes

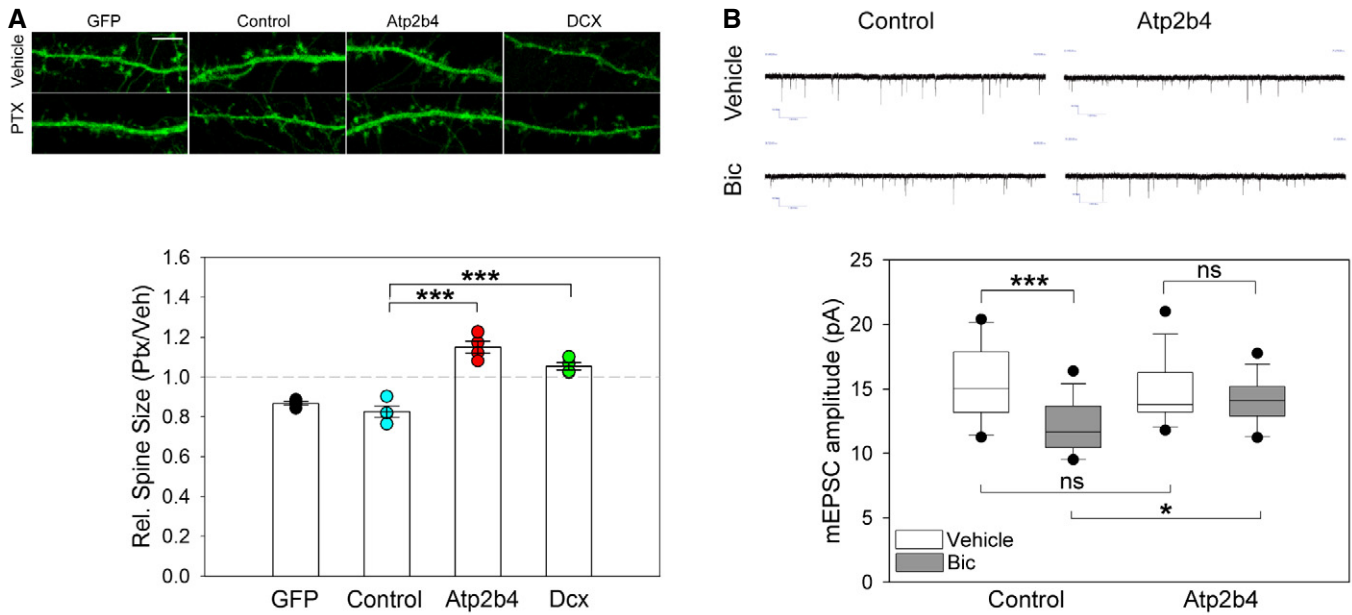


Figure 6. Downregulation of Atp2b4 is required for synaptic downscaling *in vitro*.

A Analysis of spine size when Atp2b4 or Dcx were overexpressed during PTX application. Upper panel: Representative confocal microscopy images of dendritic segments from PTX- or vehicle (Veh)-treated hippocampal neurons transfected with indicated overexpression vectors and eGFP (control = Creb-dMVP16, scale bar = 5 μ m). Bottom panel: Quantification of dendritic spine size from four independent experiments. Dot-plot presentation with mean relative spine size (PTX/Veh) \pm s.e.m. ($n = 4$; 8 neurons, \sim 200 spines/neuron per experimental condition; one-way ANOVA; $F(2,9) = 39.376$, $P < 0.001$; groups were compared by Bonferroni *post hoc* test; Contr vs. Atp2b4 $***P < 0.001$; Contr vs. Dcx $***P = 0.001$).

B Upper panel: Representative traces of mEPSC recordings from bicuculline (Bic)- or vehicle-treated neurons transfected with Atp2b4 or control expression vector. Bottom panel: Quantification of mEPSC amplitudes. Data are presented as box plots (control Veh/Bic $n = 14/16$; Atp2b4 Veh/Bic $n = 13/16$; GLM model; activity $P = 0.001$; overexpression \times activity $P = 0.048$; estimated means of specific experimental conditions were compared by pairwise comparison in SPSS; Control protein Veh vs. Bic $***P < 0.001$, Control protein Bic vs. Atp2b4 Bic $*P = 0.022$, Veh Control protein vs. Atp2b4 $P = 0.561$, Atp2b4 Veh vs. Bic $P = 0.348$).

compared to PTX-increased proteins or mRNAs (Fig 7B; Tables EV10 and EV11). This effect was particularly pronounced for highly conserved binding sites, implying a functional importance. *Atp2b4* and *Dcx* were also among the genes containing conserved Rbfox binding motifs in their 3'UTRs (Fig 7C), suggesting that they could be direct Rbfox targets. In support of this, Rbfox1 knockdown using a previously published Rbfox1-specific small interfering RNA (Hu *et al*, 2013) significantly reduced Atp2b4 and Dcx protein expression (Fig 7D). Furthermore, shRNA-mediated Rbfox1 knockdown significantly reduced the activity of Atp2b4-luc and Dcx-luc (Fig 7E), suggesting that Rbfox1 exerts its positive regulatory function via 3'UTR sequences. Taken together, these results demonstrate that Rbfox1 promotes the expression of PTX-responsive genes, such as *Atp2b4* and *Dcx* in conditions of normal neuronal activity.

Functional crosstalk between Rbfox1/3 and miR-129-5p during scaling

We next explored how the positive gene regulatory function of Rbfox can be reversed in high activity conditions that induce synaptic downscaling. Using Western blot, we found that the expression of Rbfox1 and its paralogue Rbfox3 (Fig 8A) was significantly reduced in PTX-treated neurons compared to controls. Intriguingly, inspection of the 3'UTRs of *Rbfox1* and *Rbfox3* revealed the presence of multiple miR-129-5p binding sites, some of which with high

degree of conservation (Fig 8B). This suggested that miR-129-5p could be involved in PTX-dependent downregulation of Rbfox1/3. Indeed, miR-129-5p overexpression led to a reduction in endogenous Rbfox1/3 protein expression, suggesting that Rbfox1/3 are targets of miR-129-5p (Fig 8C). To test whether repression of Rbfox proteins by miR-129-5p is mediated by miR-129-5p sites in the 3'UTR, we performed luciferase assays, focusing on *Rbfox1*. We used reporters containing either a full-length wt *Rbfox1* 3'UTR or an *Rbfox1* 3'UTR in which the two highly conserved miR-129-5p sites were mutated (129 Mut; Fig 8B). Whereas co-transfection of miR-129-5p mimics significantly repressed expression of the Rbfox1-luc wt reporter, it had no significant effect on Rbfox1-luc 129 Mut (Fig 8D). This result indicates that miR-129-5p-dependent repression of Rbfox1 is largely mediated by two highly conserved binding sites within the *Rbfox1* 3'UTR. We next explored the contribution of endogenous miR-129-5p to Rbfox1 repression. PTX treatment significantly repressed the expression of the Rbfox1-luc wt reporter (Fig 8E), but not Rbfox1-luc 129 Mut. These results suggest that endogenous miR-129-5p represses *Rbfox1* during synaptic scaling via two highly conserved sites in the 3'UTR. However, mutating the two highly conserved miR-129-5p binding sites was not sufficient to completely prevent Rbfox1 repression by miR-129-5p mimics (Fig 8D) or PTX (Fig 8E), suggesting that additional miR-129-5p binding sites might be involved. Furthermore, anti-miR-129-5p fully rescued the PTX-dependent reduction in endogenous Rbfox1 protein

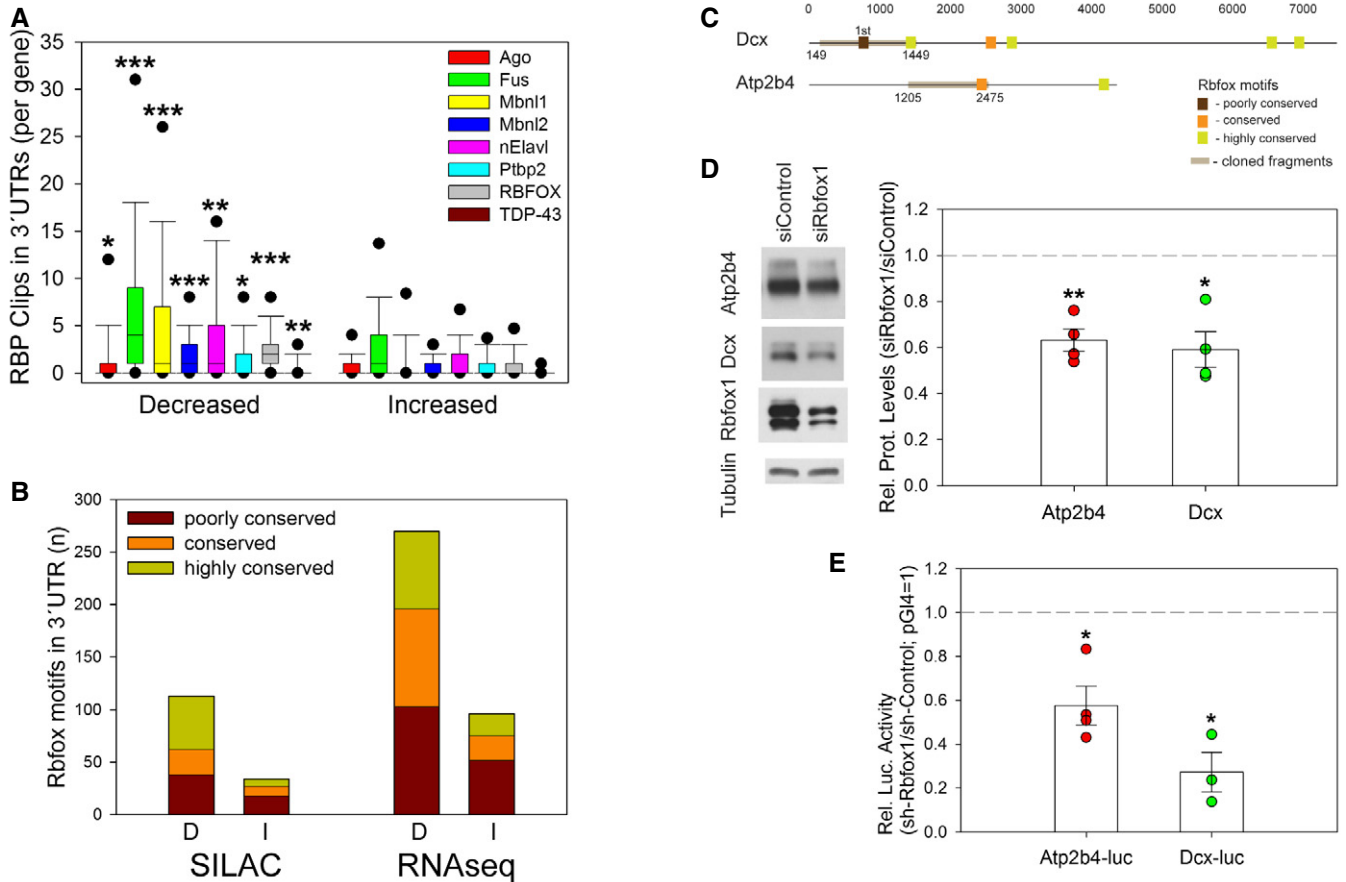


Figure 7. Rbfox1 is a positive regulator of Atp2b4 and Dcx expression.

- A** Bioinformatic analysis of published CLIP experiments for indicated RBPs performed in mouse brains. Average number of RBP CLIP tags in 3'UTRs of genes corresponding to proteins whose synthesis is increased or decreased in PTX-treated neurons (Mann–Whitney *U*-test; **P* = 0.016 (Ago); ****P* = 0.004 (nElavl); **P* = 0.010 (Ptbp2); ****P* = 0.005 (TDP-43); ****P* < 0.001).
- B** Abundance of Rbfox binding motifs (GCAUG/UGCAUG) in 3'UTRs corresponding to genes with PTX-decreased (D) or PTX-increased (I) protein synthesis (Fig 4D) or mRNA levels (Fig 4A) according to TargetScan-Human version 6.2. Seeds were classified as poorly conserved (≤ 3 species), conserved (4–9 species), or highly conserved (≥ 10 species). Bars represent total number of binding motifs per group.
- C** Localization of Rbfox binding motifs in the 3'UTRs of *Atp2b4* and *Dcx*. Motifs were classified as poorly conserved, conserved, or highly conserved as described in (B).
- D** Western blot analysis of Atp2b4, Dcx, and Rbfox1 protein expression in hippocampal neurons transfected with siRbfox1 or siControl. Left: Representative Western blot. Tubulin was used as a loading control. Right: Quantification of four independent experiments. Dot-plot presentation with mean relative protein levels (siRbfox1/siControl) normalized to tubulin \pm s.e.m. (Atp2b4, Dcx *n* = 4; independent one-sample *t*-test, two-tailed, heteroscedastic variance; Atp2b4 ***P* = 0.005, Dcx **P* = 0.013).
- E** Luciferase reporter gene assay in shRNA-Rbfox1- or shRNA-Control-transfected hippocampal neurons co-transfected with the *Dcx* or *Atp2b4* 3'UTR reporter constructs (Fig 5D). Dot-plot presentation with mean relative Luciferase activity (shRbfox1/shControl) \pm s.e.m. pGI4 (shRbfox1/shControl) was set to 1 (*n* = 3 for Dcx-luc; *n* = 4 for Atp2b4-luc; independent one-sample *t*-test, two-tailed, heteroscedastic variance; Atp2b4-luc **P* = 0.017, Dcx-luc **P* = 0.015).

Source data are available online for this figure.

(Fig 8F), confirming that miR-129-5p is required for Rbfox1 down-regulation during scaling.

Given the functional crosstalk between miR-129-5p and Rbfox1, we determined the degree of overlap between miR-129-5p and Rbfox binding motifs in the 3'UTR of PTX-downregulated genes (Fig 8G). Intriguingly, almost all miR-129-5p targets also contain at least one potential Rbfox binding site (e.g., *Atp2b4*, *Dcx*). In addition, a large group of PTX-downregulated genes are Rbfox targets (~28%) that lack consensus miR-129-5p seed matches (e.g., *Gria2*, *Atp2b3*). Therefore, by repressing Rbfox, miR-129-5p might increase its regulatory potential and in this way contribute to the suppression of up to 50% of PTX-repressed proteins.

Discussion

A miR-129-5p/Rbfox1 module coordinates the repression of synaptic genes during synaptic downscaling

Using a systematic analysis of small RNAs (Fig 1B), mRNAs (Fig 4A), and protein synthesis (Fig 4D) in combination with bioinformatics (Figs 4G and H, 7A and B, and 8G), we revealed extensive post-transcriptional regulation orchestrated by miRNAs and RBPs during homeostatic downscaling. By focusing on miRNA-dependent gene regulation, we characterized the activity-regulated miR-129-5p in more detail. miR-129-5p is upregulated by PTX, and a high

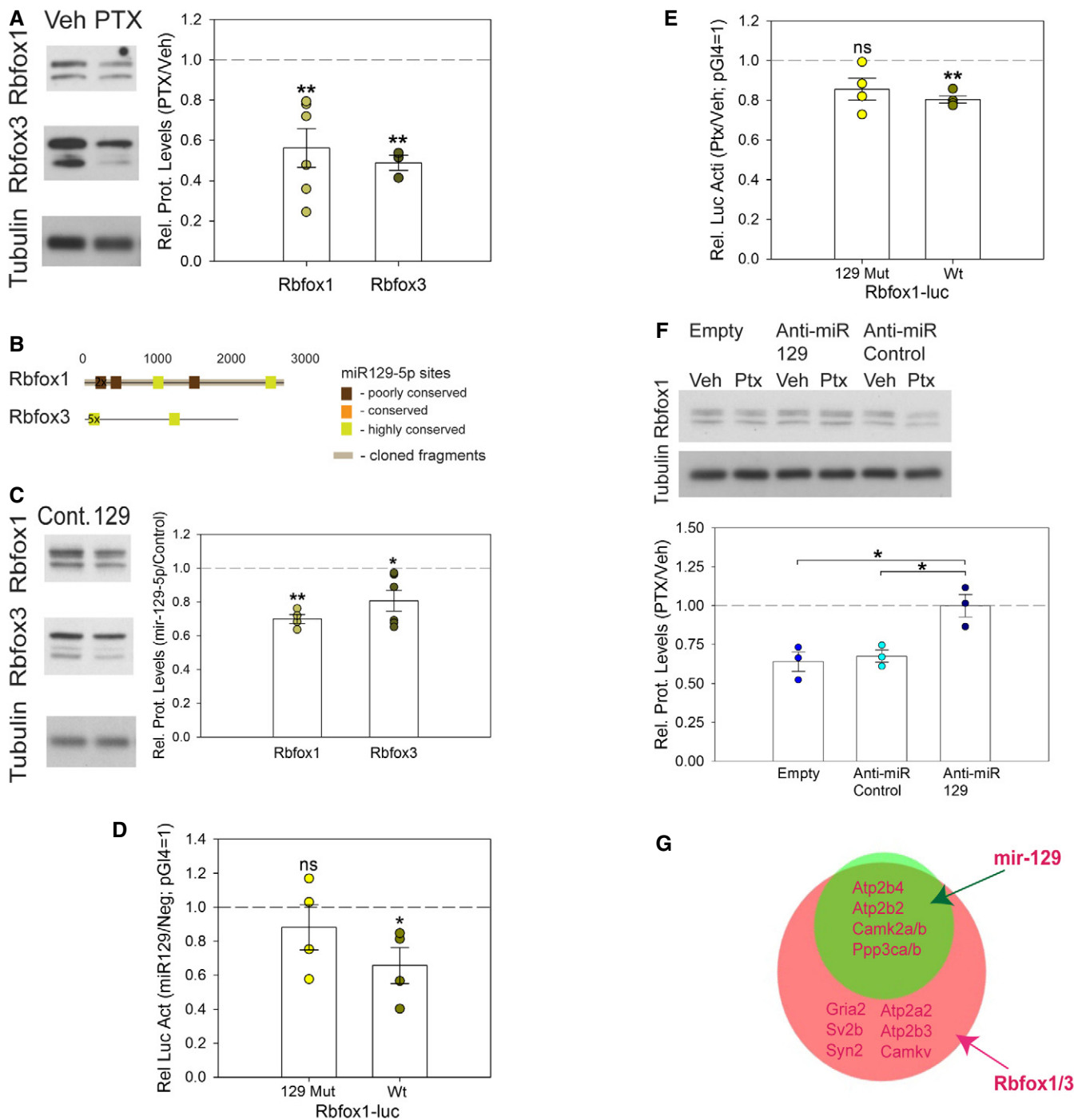


Figure 8.

number of its seed matches are localized within the 3'UTR of down-regulated genes. miR-129-5p likely works in conjunction with other activity-regulated miRNAs, including miR-134-5p, miR-132/212, miR-495, and miR-543-3p (Figs 1B and 4H, and Table EV1). For example, a number of PTX-downregulated synaptic genes contain miR-134-5p binding sites (e.g., *Dcx* (2x), *Camk2a*, *Ncald*). A systematic mutation of binding sites for PTX-regulated miRNAs together with the use of anti-miR cocktails should help to decipher the "miRNA code" involved in synaptic downscaling. In addition, we

found that miR-129-5p inhibits *Rbfox1/3* expression in a 3'UTR-dependent manner. This suggests that miR-129-5p employs at least two mechanisms that work in concert to dampen the expression of synaptic genes during PTX-induced scaling (Appendix Fig S6F). First, it directly represses mRNAs containing miR-129-5p seed matches in their 3'UTR, for example, *Atp2b4* and, to a lesser extent, *Dcx*. Second, it indirectly inhibits the expression of *Rbfox1/3* targets lacking canonical miR-129-5p binding sites (e.g., *Gria2*) by interfering with *Rbfox1/3* synthesis. Since the vast majority of miR-129-5p

Figure 8. Rbfox1/3 proteins are downregulated by PTX and miR-129-5p.

- A Western blot analysis of Rbfox1 and Rbfox3 expression in lysates from vehicle (Veh)- and PTX (48 h)-treated hippocampal neurons. Left: Representative Western blot. Tubulin was used as a loading control. Right: Quantification of multiple independent experiments. Dot-plot presentation with mean relative protein levels (PTX/Veh) normalized to tubulin \pm s.e.m. (Rbfox1 $n = 6$; Rbfox3 $n = 3$; independent one-sample t -test, two-tailed, heteroscedastic variance; Rbfox1 $**P = 0.006$, Rbfox3 $**P = 0.005$).
- B Localization of miR-129-5p binding sites in the 3'UTRs of *Rbfox1/3* based on TargetScan-Human version 6.0. Color code indicates different degree of conservation as described in Fig 4H.
- C Western blot analysis of Rbfox1 and Rbfox3 protein expression in hippocampal neurons transfected with miR-129-5p or control duplex RNA. Left: Representative Western blot. Tubulin was used as a loading control. Right: Quantification of multiple independent experiments. Dot-plot presentation with mean relative protein levels (miR-129-5p/control) normalized to tubulin \pm s.e.m. (Rbfox1 $n = 4$; Rbfox3 $n = 6$; independent one-sample t -test, two-tailed, heteroscedastic variance; Rbfox1 $**P = 0.002$, Rbfox3 $*P = 0.025$).
- D Luciferase reporter gene assay in vehicle (Veh)- or PTX-treated hippocampal neurons transfected with the *Rbfox1* 3'UTR reporter construct (Rbfox1-luc) containing either wt or 129mut (2-highly conserved sites) binding sites. Dot-plot presentation with mean relative luciferase activity (miR-129-5p/control) normalized to pGL4 empty vector \pm s.e.m. ($n = 4$; independent one-sample t -test, two-tailed, heteroscedastic variance; Rbfox1-luc wt $*P = 0.0476$, Rbfox1-luc 129mut $P = 0.4428$).
- E Luciferase reporter gene assay in vehicle (Veh)- or PTX-treated hippocampal neurons transfected with the *Rbfox1*-luc containing either wt or 129mut (2-highly conserved sites) binding sites. Dot-plot presentation with mean luciferase activity (PTX/Veh) \pm s.e.m. pGL4 (PTX/Veh) was set to 1 ($n = 4$; independent one-sample t -test, two-tailed, heteroscedastic variance; Rbfox1-luc wt $**P = 0.00185$, Rbfox1-luc 129mut $P = 0.0812$).
- F Western blot analysis of Rbfox1 protein expression in PTX- or mock-treated hippocampal neurons that were transfected with the indicated anti-miRs. Upper panel: Representative Western blot. Tubulin was used as a loading control. Bottom panel: Quantification of three independent experiments. Dot-plot presentation with mean relative protein levels (PTX/Veh) \pm s.e.m. ($n = 3$; one-way ANOVA; $F(2,6) = 10.956$, $P = 0.010$; groups were compared by Bonferroni *post hoc* test; anti-miR-129-5p vs. anti-miR Cont $*P = 0.026$; anti-miR-129-5p vs. Empty $*P = 0.016$).
- G Overlap between targets that contain miR-129-5p and Rbfox binding motifs. Selected targets are indicated.

Source data are available online for this figure.

targets also contain adjacent Rbfox motifs in their 3'UTR but not vice versa (Fig 8G), removal of the positive regulator Rbfox might be the main trigger for repression. Direct miR-129-5p inhibition could then be used to further strengthen repression of specific targets. In the future, genome-wide target maps of miR-129-5p and Rbfox1 will be highly informative to fully understand the miR-129-5p/Rbfox crosstalk and its significance for synaptic scaling. The potassium channel subunit Kv1.1 was recently shown to be a direct miR-129-5p target (Sosanya et al, 2013). However, PTX-dependent upregulation of miR-129-5p was not paralleled by reduced, but rather elevated Kv1.1 mRNA levels (Table EV4). A possible explanation could be that Kv1.1 inhibition by miR-129-5p in neuronal dendrites occurs specifically at the translational level and does not involve mRNA degradation, as shown for other dendritic miRNA targets (e.g., Limk1; Schratt et al, 2006). Consistent with this hypothesis, mutation of the miR-129-5p binding site within Kv1.1 did not lead to changes in Kv1.1 mRNA levels (Sosanya et al, 2013). Since Kv1.1 was not detectable by pSILAC (Table EV7), our study does not allow any conclusions with regard to PTX-dependent regulation of Kv1.1 protein synthesis.

Post-transcriptional regulation in synaptic downscaling

In addition to the identification of specific regulatory mechanisms, our study provides support for a general importance of 3'UTR-dependent post-transcriptional regulation in synaptic downscaling. Bioinformatic analysis provides evidence that the 3'UTRs of PTX-downregulated genes were on average more than twice as long as those from PTX-upregulated genes (Fig 4G and Tables EV8 and EV9) and contain more miRNA (Fig 4H) and RBP binding motifs or CLIP peaks (Fig 7A and B). Together with previous studies that showed that mRNAs encoding synaptic proteins contain extraordinarily long 3'UTRs (Miura et al, 2013), this result suggests that genes suppressed during synaptic scaling are very susceptible to regulation at the level of mRNA translation and/or stability.

Novel players in synaptic downscaling might regulate calcium homeostasis and AMPA-R dynamics

Our comprehensive proteome and transcriptome analysis further allowed the identification of entire pathways and signaling complexes that are coordinately regulated during scaling, such as calcium-mediated signaling and glutamate receptor signaling (Fig 4B, Appendix Fig S5J). While both processes have been previously implicated in synaptic scaling, we obtained evidence for regulation of additional players within these pathways that can be functionally tested in future studies. For example, our results point to a global reduction in the neuronal calcium extrusion system (i.e., reductions in the membrane ATPases Atp2b1-4; Fig 4 and Tables EV4 and EV7), in agreement with an important function of calcium homeostasis in synaptic scaling (Turrigiano, 2012). In the context of glutamate receptor complexes, we observed robust PTX-dependent downregulation of regulators of AMPA-R dynamics, such as Mpp2/Dlg2 and Rap2b (Karnak et al, 2002; Schwenk et al, 2012). Although our studies mainly focused on postsynaptic mechanisms, we also observed a downregulation of crucial presynaptic proteins (e.g., Synj1, Ncald, Syn1/2) during scaling, which is in agreement with previous studies (Davis & Muller, 2015).

Post-transcriptional regulation of synaptic downscaling in epileptogenesis

Concerning pathophysiological significance, intriguing links between homeostatic plasticity and epilepsy-causing channelopathies exist (Frank, 2014). Nevertheless, it is still debated whether homeostatic plasticity is protective or maladaptive in the context of epilepsy (Swann & Rho, 2014). Our results are more consistent with a maladaptive role of homeostatic plasticity in epilepsy. First, antagonism of miR-129-5p and miR-134-5p, two miRNAs that we found to be required for synaptic scaling (Fig 2; Fiore et al, 2014), prevent the development and progression of

epileptic seizures (Fig 3; Jimenez-Mateos *et al* 2012). Second, loss-of-function mouse models for several PTX-downregulated genes [e.g., *Dcx/Dcl2* (Kerjan *et al*, 2009), *Bsn* (Altrock *et al*, 2003), *Rbfox1* (Gehman *et al*, 2011)] display increased seizure susceptibility. Third human loss-of-function mutations in PTX-downregulated genes (e.g., *SYNGAP1*, *Rbfox1*) have been associated with epilepsy (Carvill *et al*, 2013; Lal *et al*, 2013; Frank, 2014). By inference, antagonizing PTX-upregulated miRNAs, such as miR-129-5p, might represent a promising strategy for therapeutic intervention in epilepsy.

Materials and Methods

Animal experiments

All animal experiments were performed in accordance with the European Communities Council Directive (2010/63/EU) and ARRIVE guidelines. Please see Appendix Supplementary Methods for further details.

Perforant pathway stimulation paradigms

Rats were implanted bilaterally with unipolar stainless steel recording electrodes in the dentate granule cell layer of the dorsal hippocampus and with bipolar stimulating electrodes in the angular bundles of the perforant pathway. Please see Appendix Supplementary Methods for further details.

Electrophysiological and video monitoring methods

Immediately following perforant pathway stimulation (PPS), intracranial EEG was recorded continuously (24/7) from the left dentate gyrus via the implanted EEG transmitter. In addition, continuous video recordings were performed for each rat using network cameras (Edimax Technology, Willich, Germany). The complete EEG recording was visually evaluated for seizure activity by a trained researcher using NeuroArchiver software (Open Source Instruments, Watertown, MA, USA). Each confirmed electrographic seizure was related to behavior on the time-stamped video recordings.

Perfusion-fixation and tissue treatment

At different time points (1, 24, 72 h, 10 and 16 days after the final PPS as well as 1 and 30 days after the first spontaneous seizure; 17 days after electrode implantation for control animals; $n = 3$ per group), rats were deeply anesthetized with ketamine (100 mg/kg i.p.) and xylazine (15 mg/kg i.p.) and perfused through the aorta by gravity feed with ice-cold saline for 2 min. After perfusion, brains were quickly removed from the skull. The hippocampi were dissected on ice, immediately snap-frozen on dry ice and stored at -80°C .

Ago2-IP and small RNA-seq

Rat dentate gyrus was homogenised in RNase-free IP buffer (300 mM NaCl, 5 mM MgCl_2 , 0.1% NP-40, 50 mM Tris-HCl pH 7.5,

protease, and RNase inhibitor). Cell lysate was pre-cleared using protein A/G beads (Santa Cruz Biotechnology), and Ago-2 antibody (Cell Signaling, Cat. #2897) was added and allowed to incubate overnight at 4°C , after which A/G agarose beads were added and allowed to incubate for 2 h at 4°C . Ago2-immunoprecipitated RNA was purified from pelleted beads using Trizol/chloroform purification. Please see Appendix Supplementary Methods for further details.

Silencing of miR-129-5p in naive mice

Mice ($n = 3/4$ per group) underwent surgical procedure under anesthesia (isoflurane; 5% induction, 1–2% maintenance) in a mouse adapted stereotaxic frame. Body temperature was maintained within the normal physiological range with a feedback-controlled heat pad (Harvard Apparatus, Kent, UK; Holliston, MA). After a midline scalp incision, partial craniectomies were performed. One guide cannula (Plastic Ones Inc.) was implanted to allow intracerebroventricular (i.c.v.) injection. This cannulas was placed on the dura mater with the following coordinates from bregma: AP = +0.3 mm, L = +0.9 mm. After recovery from surgery, mice were randomly injected (i.c.v.) with 0.5 nmol/2 μl locked nucleic acid (LNA) oligonucleotide targeting miR-129-5p (anti-miR-129-5p) or control (PBS). Twenty-four hours later, mice were deeply anesthetized (pentobarbital) and transcardially perfused (PBS). Ipsilateral hippocampi were removed to assess the levels of miR-129-5p by qPCR.

Focal-onset status epilepticus in mice

A second cohort of mice ($n = 5/\text{group}$) were equipped for EEG recordings under surgical anesthesia in a mouse adapted stereotaxic frame, as previously described. Animals had skull-mounted recording electrodes placed and fixed with dental cement. Two guide cannulas (Plastic Ones Inc.) were also implanted to allow intracerebroventricular (i.c.v.) and intra-amygdala (i.a.) injections. Please see Appendix Supplementary Methods for further details.

EEG and behavior analysis

Mouse EEG data were analyzed and quantified using LabChart 8 software (ADInstruments, Oxford, UK) by a reviewer blind to treatment. Please see Appendix Supplementary Methods for further details.

Histopathology

Irreversible neuronal injury was assessed using Fluoro-Jade B (FJB) (Millipore), as described (Jimenez-Mateos *et al*, 2012). Please see Appendix Supplementary Methods for further details.

DNA constructs

Please see Appendix Supplementary Methods for further details.

Cell culture, transfection, and stimulation

Primary cultures of Sprague Dawley rats (Charles River Laboratories, Sulzfeld, Germany) embryonic hippocampal (HC) and cortical

neurons (Ctx) were done as described previously (Schratt *et al*, 2006). Please see Appendix Supplementary Methods for further details.

Luciferase reporter assay

Primary neurons were transfected in triplicate in 24-well plates using for each well 100 ng of pGL4 firefly reporter constructs and equal amounts of empty Renilla reporter as transfection control, alone or with respective miRNA mimics (Ambion® Pre-miR™ miRNA Precursor: miR-129-5p, Neg-Control1). Luciferase assays (overexpression/activity experiments) were performed 4 days post-transfection using the Dual-Luciferase reporter assay system (Baker & Boyce, 2014) on a GloMax R96 Microplate Luminometer (Promega).

Bicistronic reporter assay

Hippocampal neurons (13 DIV) were transfected with 150 ng of bicistronic reporter constructs (pTracer-CMV-dsRED, 50 ng) and 50 ng of EGFP vector together with the indicated anti-miRs (pLNAs—Exiqon). Cells were analyzed at 20 DIV. pTracer-129-5p-sensor contains two copies of a perfect binding site for miR-129-5p in the 3'UTR of dsRED, which leads to degradation of the dsRED RNA in the presence of miR-129-5p. Cells in which the dsRED signal did not exceed background levels were scored as “miRNA positive”.

Image analysis

All image analysis was performed with the scientist blinded to the experimental conditions. Please see Appendix Supplementary Methods for further details.

Single molecule fluorescence *in situ* hybridization (smFISH)

Dissociated hippocampal neurons were fixed at 20 DIV using 4% paraformaldehyde/4% sucrose/PBS for 30 min at room temperature. FISH was performed using the QuantiGene (QG) ViewRNA kit (Affymetrix) according to the manufacturer's protocol using probes for *Camk2a*, *Dcx*, and *Atp2b4*. Please see Appendix Supplementary Methods for further details.

Preparation of protein extracts and Western blot

A total of 2.7 million hippocampal cells were plated on one 6-well plate and treated with fluorodeoxyuridine (FUdR; Sigma; F-0503) + uridine (Sigma; F-303) (final concentration 10 μ M) from 3 DIV to stop proliferation of non-neuronal cells. At 20 DIV, neuronal enriched cultures were washed once with warm DPBS (Invitrogen). Afterward, modified RIPA buffer (50 mM Tris-HCl, 150 mM NaCl, 0.5% NP-40, 0.1% SDS, pH 7.4) containing Complete Protease Inhibitor Cocktail EDTA-free (Roche) was added. Please see Appendix Supplementary Methods for further details.

Cross-linking assay for measuring GluA1 cell surface expression

To be able to differentiate between surface and intracellularly expressed GluA1 by SDS-PAGE and immunoblotting, we used a

modified protein cross-linking assay developed by Boudreau *et al* (2012). Please see Appendix Supplementary Methods for further details.

Electrophysiology

Miniature excitatory postsynaptic currents (mEPSCs) were recorded in whole-cell voltage-clamp mode using an EPC-10 patch-clamp amplifier and PATCHMASTER software (HEKA Elektronik, Lambrecht, Germany). Dissociated hippocampal neurons were transfected at 12 DIV with corresponding plasmids or anti-miRs (pLNAs; Exiqon). Bicuculline (20 μ M) was applied on 18–19 DIV for 48 h before cells were transferred to the bath solution on 20–21 DIV. Please see Appendix Supplementary Methods for further details.

Pulsed SILAC labeling of primary hippocampal neuronal cells

Analysis of arginine-6 and lysine-D4 incorporation rates

At 10 DIV, Neurobasal medium without arginine and lysine was added to FUdR-treated HC (1:1 dilution with “old” medium). Media containing arginine-6/lysine-D4 (final conc. 200 μ M/400 μ M; + proline 1.72 mM) was added to the cells at 12, 13, 14, 15, 16, and 17 DIV. Non-labeled proline was used to prevent arginine to proline conversion. At 18 DIV, proteins were extracted with modified RIPA buffer (150 mM NaCl, 50 mM Tris-HCl pH 7.4, 0.5% NP-40, 0.1% SDS), measured, and processed as described in Nolte *et al* (2015). Please see Appendix Supplementary Methods for further details.

SILAC labeling for protein quantification

Arginine-10 (200 μ M), lysine-8 (400 μ M), and non-labeled proline (1.72 mM) were applied to neuronal cells 4 h after plating for 20–27 days. Almost 90% SILAC labeling was achieved after 20 days (Table EV5), and those labeled proteins were used as SILAC spike-in to accurately quantify protein abundances of non-labeled (pre-existing) and arginine-6/lysine-D4-labeled (newly synthesized) proteins in primary neuronal cells (Geiger *et al*, 2010).

PTX experiment

Neuronal enriched cultures were fed without Arg/Lys from 9 DIV (to dilute the non-labeled arginine and lysine). Decrease in non-labeled arginine and lysine concentration in the medium did not have obvious effect on cell morphology and viability. At 15 DIV, Arg6/LysD4 (200 μ M/400 μ M; + Pro at 1.72 mM) was added to the medium. PTX was applied at 18 DIV for 48 h. At 20 DIV, proteins were extracted and concentration measured as described earlier. Samples were mixed 1:1 with neuronal spike-in standard and separated by 1D SDS-PAGE gel electrophoresis (Bio-Rad). Please see Appendix Supplementary Methods for further details.

RNA extraction

RNA was extracted from FUdR-treated HC using peqGOLD Isolation Systems TriFast™ (Peqlab) following the manufacturer's protocol. To remove potential DNA contamination, RNA samples were treated with TURBO™ DNase (Ambion) and RNA was re-extracted as described before. Samples were stored at -80° C until further use. For *in vivo* experiments with anti-miR-129-5p application, total RNA

was isolated from brain samples using Trizol (Invitrogen), as described previously (Jimenez-Mateos *et al*, 2012).

Quantitative real-time PCR

RNA was reverse-transcribed with SuperScript[®] III Reverse Transcriptase (Invitrogen) using random hexamers (total RNA) or oligo dT₂₀ primers (poly-RNA) according to manufacturer's instructions. Quantitative real-time PCR was performed with the StepOnePlus Real-Time PCR System (Applied Biosystems), using iTaq SYBR Green Supermix with ROX (Bio-Rad) for detection of mRNA and TaqMan MicroRNA Assay kits (Applied Biosystems) for detection of mature miRNAs (miR-132-3p, miR-129-5p). Please see Appendix Supplementary Methods for further details.

Small RNA-seq

Small RNA libraries were constructed and sequenced by the EMBL genomic core facility (Heidelberg, Germany). Please see Appendix Supplementary Methods for further details.

PolyA RNA-seq

PolyA RNA sequencing was performed by EMBL genomic core facility (Heidelberg, Germany).

Bioinformatic analysis

Please see Appendix Supplementary Methods for a detailed description of bioinformatic approaches (mapping; differential gene expression; 3'UTR length estimation; miRNA and Rbfox motif analysis; GO term enrichment; CLIP analysis).

Statistics

Unless otherwise stated, three independent experiments were performed for each data set. Detailed information about statistics for each figure is in Table EV12. Please see Appendix Supplementary Methods for further details.

Data access

The mass spectrometry proteomics data have been deposited to the ProteomeXchange Consortium via the PRIDE partner repository (Vizcaino *et al*, 2016) with the dataset identifier PXD004150. Data from RNA-seq experiments were submitted to the GEO repository with the dataset identifier GSE81437.

Expanded View for this article is available online.

Acknowledgements

We thank J.D. Richter and M.E. Greenberg for providing reagents. We thank R. Fiore and A. Antoniou for comments on the manuscript. We thank E. Becker, R. Gondrum, U. Beck and B. Kowalski for excellent technical assistance. This work was supported by grants from the EU (ERC Starting Grant "Neuromir"; FP7 "EpimiRNA" No. 602130) and the DFG (SPP1738; FOR2107; SCHR 1136/8-1) to G.S. as well as DFG FI 2157/2-1 to R.F. S.Bi. is a recipient of a grant from the Von Behring-Röntgen-Stiftung (62-0004).

Author contributions

MR designed and performed most of the experiments, analyzed the data, and wrote the manuscript. FM and CD analyzed data from RNA-seq experiments and performed integrative bioinformatic analyses. RF performed and analyzed spine experiments. SK analyzed data from small RNA sequencing. AA-A performed and analyzed patch-clamp recordings. CRR performed *in vivo* rescue experiments with anti-miR-129. S.Bi performed and analyzed FISH experiments. S.Ba, BN, and FR performed rat PPS. MTV and JK performed Ago2-IP and analyzed small RNA-seq. MK and TB supervised mass spectrometry analysis. RR and GB processed the human samples and ran the qPCR. ND performed patient recruitment. MF performed tissue preparation and hippocampal sclerosis grading. DO performed operations of human TLE patients. DH supervised the human epilepsy study. GS wrote the manuscript and coordinated the entire project.

Conflict of interest

The authors declare that they have no conflict of interest.

References

- Altrock WD, tom Dieck S, Sokolov M, Meyer AC, Sigler A, Brakebusch C, Fassler R, Richter K, Boeckers TM, Potschka H, Brandt C, Loscher W, Grimberg D, Dresbach T, Hempelmann A, Hassan H, Balschun D, Frey JU, Brandstatter JH, Garner CC *et al* (2003) Functional inactivation of a fraction of excitatory synapses in mice deficient for the active zone protein bassoon. *Neuron* 37: 787–800
- Baker JM, Boyce FM (2014) High-throughput functional screening using a homemade dual-glow luciferase assay. *J Vis Exp* 88: e50282
- Bartel DP (2009) MicroRNAs: target recognition and regulatory functions. *Cell* 136: 215–233
- Boudreau AC, Milovanovic M, Conrad KL, Nelson C, Ferrario CR, Wolf ME (2012) A protein cross-linking assay for measuring cell surface expression of glutamate receptor subunits in the rodent brain after *in vivo* treatments. *Curr Protoc Neurosci* Chapter 5: Unit 5.30.31-19
- Carvill GL, Heavin SB, Yendle SC, McMahon JM, O'Roak BJ, Cook J, Khan A, Dorschner MO, Weaver M, Calvert S, Malone S, Wallace G, Stanley T, Bye AM, Bleasel A, Howell KB, Kivity S, Mackay MT, Rodriguez-Casero V, Webster R *et al* (2013) Targeted resequencing in epileptic encephalopathies identifies *de novo* mutations in CHD2 and SYNGAP1. *Nat Genet* 45: 825–830
- Charizanis K, Lee KY, Batra R, Goodwin M, Zhang C, Yuan Y, Shiue L, Cline M, Scotti MM, Xia G, Kumar A, Ashizawa T, Clark HB, Kimura T, Takahashi MP, Fujimura H, Jinnai K, Yoshikawa H, Gomes-Pereira M, Gourdon G *et al* (2012) Muscleblind-like 2-mediated alternative splicing in the developing brain and dysregulation in myotonic dystrophy. *Neuron* 75: 437–450
- Chi SW, Zang JB, Mele A, Darnell RB (2009) Argonaute HITS-CLIP decodes microRNA-mRNA interaction maps. *Nature* 460: 479–486
- Cohen JE, Lee PR, Chen S, Li W, Fields RD (2011) MicroRNA regulation of homeostatic synaptic plasticity. *Proc Natl Acad Sci USA* 108: 11650–11655
- Colombrita C, Silani V, Ratti A (2013) ELAV proteins along evolution: back to the nucleus? *Mol Cell Neurosci* 56: 447–455
- Davis GW, Muller M (2015) Homeostatic control of presynaptic neurotransmitter release. *Annu Rev Physiol* 77: 251–270
- Decembrini S, Bressan D, Vignali R, Pitto L, Mariotti S, Rainaldi G, Wang X, Evangelista M, Barsacchi G, Cremisi F (2009) MicroRNAs couple cell fate and developmental timing in retina. *Proc Natl Acad Sci USA* 106: 21179–21184

- Desai NS, Cudmore RH, Nelson SB, Turrigiano GG (2002) Critical periods for experience-dependent synaptic scaling in visual cortex. *Nat Neurosci* 5: 783–789
- Diering GH, Gustina AS, Hugarir RL (2014) PKA-GluA1 coupling via AKAP5 controls AMPA receptor phosphorylation and cell-surface targeting during bidirectional homeostatic plasticity. *Neuron* 84: 790–805
- Diering GH, Nirujogi RS, Roth RH, Worley PF, Pandey A, Hugarir RL (2017) Homer1a drives homeostatic scaling-down of excitatory synapses during sleep. *Science* 355: 511–515
- Evers DM, Matta JA, Hoe HS, Zarkowsky D, Lee SH, Isaac JT, Pak DT (2010) Plk2 attachment to NSF induces homeostatic removal of GluA2 during chronic overexcitation. *Nat Neurosci* 13: 1199–1207
- Fiore R, Khudayberdiev S, Christensen M, Siegel G, Flavell SW, Kim TK, Greenberg ME, Schrott G (2009) Mef2-mediated transcription of the miR379-410 cluster regulates activity-dependent dendritogenesis by fine-tuning Pumilio2 protein levels. *EMBO J* 28: 697–710
- Fiore R, Rajman M, Schwale C, Bicker S, Antoniou A, Bruehl C, Draguhn A, Schrott G (2014) MiR-134-dependent regulation of Pumilio-2 is necessary for homeostatic synaptic depression. *EMBO J* 33: 2231–2246
- Frank CA (2014) How voltage-gated calcium channels gate forms of homeostatic synaptic plasticity. *Front Cell Neurosci* 8: 40
- Gao M, Sossa K, Song L, Errington L, Cummings L, Hwang H, Kuhl D, Worley P, Lee HK (2010) A specific requirement of Arc/Arg3.1 for visual experience-induced homeostatic synaptic plasticity in mouse primary visual cortex. *J Neurosci* 30: 7168–7178
- Gehman LT, Stoilov P, Maguire J, Damianov A, Lin CH, Shiue L, Ares M Jr, Mody I, Black DL (2011) The splicing regulator Rbfox1 (A2BP1) controls neuronal excitation in the mammalian brain. *Nat Genet* 43: 706–711
- Geiger T, Cox J, Ostasiewicz P, Wisniewski JR, Mann M (2010) Super-SILAC mix for quantitative proteomics of human tumor tissue. *Nat Methods* 7: 383–385
- Groth RD, Lindskog M, Thiagarajan TC, Li L, Tsien RW (2011) Beta Ca₂ + / CaM-dependent kinase type II triggers upregulation of GluA1 to coordinate adaptation to synaptic inactivity in hippocampal neurons. *Proc Natl Acad Sci USA* 108: 828–833
- Hou Q, Ruan H, Gilbert J, Wang G, Ma Q, Yao WD, Man HY (2015) MicroRNA miR124 is required for the expression of homeostatic synaptic plasticity. *Nat Commun* 6: 10045
- Hu J, Ho AL, Yuan L, Hu B, Hua S, Hwang SS, Zhang J, Hu T, Zheng H, Gan B, Wu G, Wang YA, Chin L, DePinho RA (2013) From the Cover: neutralization of terminal differentiation in gliomagenesis. *Proc Natl Acad Sci USA* 110: 14520–14527
- Ibata K, Sun Q, Turrigiano GG (2008) Rapid synaptic scaling induced by changes in postsynaptic firing. *Neuron* 57: 819–826
- Ince-Dunn G, Okano HJ, Jensen KB, Park WY, Zhong R, Ule J, Mele A, Fak JJ, Yang C, Zhang C, Yoo J, Herre M, Okano H, Noebels JL, Darnell RB (2012) Neuronal Elav-like (Hu) proteins regulate RNA splicing and abundance to control glutamate levels and neuronal excitability. *Neuron* 75: 1067–1080
- Ishigaki S, Masuda A, Fujioka Y, Iguchi Y, Katsuno M, Shibata A, Urano F, Sobue G, Ohno K (2012) Position-dependent FUS-RNA interactions regulate alternative splicing events and transcriptions. *Sci Rep* 2: 529
- Jimenez-Mateos EM, Bray I, Sanz-Rodriguez A, Engel T, McKiernan RC, Mouri G, Tanaka K, Sano T, Saugstad JA, Simon RP, Stallings RL, Henshall DC (2011) miRNA Expression profile after status epilepticus and hippocampal neuroprotection by targeting miR-132. *Am J Pathol* 179: 2519–2532
- Jimenez-Mateos EM, Engel T, Merino-Serrais P, McKiernan RC, Tanaka K, Mouri G, Sano T, O'Tuathaigh C, Waddington JL, Prenter S, Delanty N, Farrell MA, O'Brien DF, Conroy RM, Stallings RL, DeFelipe J, Henshall DC (2012) Silencing microRNA-134 produces neuroprotective and prolonged seizure-suppressive effects. *Nat Med* 18: 1087–1094
- Jimenez-Mateos EM, Engel T, Merino-Serrais P, Feraud-Espinosa I, Rodriguez-Alvarez N, Reynolds J, Reschke CR, Conroy RM, McKiernan RC, deFelipe J, Henshall DC (2015) Antagomirs targeting microRNA-134 increase hippocampal pyramidal neuron spine volume *in vivo* and protect against pilocarpine-induced status epilepticus. *Brain Struct Funct* 220: 2387–2399
- Karnak D, Lee S, Margolis B (2002) Identification of multiple binding partners for the amino-terminal domain of synapse-associated protein 97. *J Biol Chem* 277: 46730–46735
- Kedde M, Agami R (2008) Interplay between microRNAs and RNA-binding proteins determines developmental processes. *Cell Cycle* 7: 899–903
- Kerjan G, Koizumi H, Han EB, Dube CM, Djakovic SN, Patrick GN, Baram TZ, Heinemann SF, Gleeson JG (2009) Mice lacking doublecortin and doublecortin-like kinase 2 display altered hippocampal neuronal maturation and spontaneous seizures. *Proc Natl Acad Sci USA* 106: 6766–6771
- Kim S, Ziff EB (2014) Calcineurin mediates synaptic scaling via synaptic trafficking of Ca²⁺-permeable AMPA receptors. *PLoS Biol* 12: e1001900
- Lal D, Trucks H, Moller RS, Hjalgrim H, Koeleman BP, de Kovel CG, Visscher F, Weber YG, Lerche H, Becker F, Schankin CJ, Neubauer BA, Surges R, Kunz WS, Zimprich F, Franke A, Illig T, Ried JS, Leu C, Nurnberg P et al (2013) Rare exonic deletions of the RFX1 gene increase risk of idiopathic generalized epilepsy. *Epilepsia* 54: 265–271
- Lee JA, Damianov A, Lin CH, Fontes M, Parikhshak NN, Anderson ES, Geschwind DH, Black DL, Martin KC (2016) Cytoplasmic Rbfox1 regulates the expression of synaptic and autism-related genes. *Neuron* 89: 113–128
- Letellier M, Eramah S, Mondin M, Soula A, Penn A, Choquet D, Landry M, Thoumine O, Favereaux A (2014) miR-92a regulates expression of synaptic GluA1-containing AMPA receptors during homeostatic scaling. *Nat Neurosci* 17: 1040–1042
- Li Z, Zhang Y, Ku L, Wilkinson KD, Warren ST, Feng Y (2001) The fragile X mental retardation protein inhibits translation via interacting with mRNA. *Nucleic Acids Res* 29: 2276–2283
- Licalosi DD, Yano M, Fak JJ, Mele A, Grabinski SE, Zhang C, Darnell RB (2012) Ptpb2 represses adult-specific splicing to regulate the generation of neuronal precursors in the embryonic brain. *Genes Dev* 26: 1626–1642
- Lovci MT, Ghanem D, Marr H, Arnold J, Gee S, Parra M, Liang TY, Stark TJ, Gehman LT, Hoon S, Massier KB, Pratt GA, Black DL, Gray JW, Conboy JG, Yeo GW (2013) Rbfox proteins regulate alternative mRNA splicing through evolutionarily conserved RNA bridges. *Nat Struct Mol Biol* 20: 1434–1442
- Martin KC, Ephrussi A (2009) mRNA localization: gene expression in the spatial dimension. *Cell* 136: 719–730
- McKiernan RC, Jimenez-Mateos EM, Sano T, Bray I, Stallings RL, Simon RP, Henshall DC (2012) Expression profiling the microRNA response to epileptic preconditioning identifies miR-184 as a modulator of seizure-induced neuronal death. *Exp Neurol* 237: 346–354
- Miura P, Shenker S, Andreu-Agullo C, Westholm JO, Lai EC (2013) Widespread and extensive lengthening of 3' UTRs in the mammalian brain. *Genome Res* 23: 812–825
- Nolte H, Holper S, Housley MP, Islam S, Piller T, Konzer A, Stainier DY, Braun T, Kruger M (2015) Dynamics of zebrafish fin regeneration using a pulsed SILAC approach. *Proteomics* 15: 739–751
- Norwood BA, Bauer S, Wegner S, Hamer HM, Oertel WH, Sloviter RS, Rosenow F (2011) Electrical stimulation-induced seizures in rats: a “dose-response” study on resultant neurodegeneration. *Epilepsia* 52: e109–e112

- Paschou M, Paraskevopoulou MD, Vlachos IS, Koukouraki P, Hatzigeorgiou AG, Doxakis E (2012) miRNA regulons associated with synaptic function. *PLoS One* 7: e46189
- Polymenidou M, Lagier-Tourenne C, Hutt KR, Huelga SC, Moran J, Liang TY, Ling SC, Sun E, Wancewicz E, Mazur C, Kordasiewicz H, Sedaghat Y, Donohue JP, Shiue L, Bennett CF, Yeo GW, Cleveland DW (2011) Long pre-mRNA depletion and RNA missplicing contribute to neuronal vulnerability from loss of TDP-43. *Nat Neurosci* 14: 459–468
- Remenyi J, Hunter CJ, Cole C, Ando H, Impey S, Monk CE, Martin KJ, Barton GJ, Hutvagner G, Arthur JS (2010) Regulation of the miR-212/132 locus by MSK1 and CREB in response to neurotrophins. *Biochem J* 428: 281–291
- Schratt GM, Tuebing F, Nigh EA, Kane CG, Sabatini ME, Kiebler M, Greenberg ME (2006) A brain-specific microRNA regulates dendritic spine development. *Nature* 439: 283–289
- Schratt G (2009) microRNAs at the synapse. *Nat Rev Neurosci* 10: 842–849
- Schwenk J, Harmel N, Brechet A, Zolles G, Berkefeld H, Muller CS, Bildl W, Baehrens D, Huber B, Kulik A, Klocker N, Schulte U, Fakler B (2012) High-resolution proteomics unravel architecture and molecular diversity of native AMPA receptor complexes. *Neuron* 74: 621–633
- Selbach M, Schwanhaussner B, Thierfelder N, Fang Z, Khanin R, Rajewsky N (2008) Widespread changes in protein synthesis induced by microRNAs. *Nature* 455: 58–63
- Shepherd JD, Rumbaugh G, Wu J, Chowdhury S, Plath N, Kuhl D, Huganir RL, Worley PF (2006) Arc/Arg3.1 mediates homeostatic synaptic scaling of AMPA receptors. *Neuron* 52: 475–484
- Siddoway B, Hou H, Xia H (2014) Molecular mechanisms of homeostatic synaptic downscaling. *Neuropharmacology* 78: 38–44
- Sosanya NM, Huang PP, Cacheaux LP, Chen CJ, Nguyen K, Perrone-Bizzozero NI, Raab-Graham KF (2013) Degradation of high affinity HuD targets releases Kv1.1 mRNA from miR-129 repression by mTORC1. *J Cell Biol* 202: 53–69
- Strehler EE, Filoteo AG, Penniston JT, Caride AJ (2007) Plasma-membrane Ca(2+) pumps: structural diversity as the basis for functional versatility. *Biochem Soc Trans* 35: 919–922
- Su W, Aloisi MS, Garden GA (2016) MicroRNAs mediating CNS inflammation: small regulators with powerful potential. *Brain Behav Immun* 52: 1–8
- Swann JW, Rho JM (2014) How is homeostatic plasticity important in epilepsy? *Adv Exp Med Biol* 813: 123–131
- Turrigiano G (2012) Homeostatic synaptic plasticity: local and global mechanisms for stabilizing neuronal function. *Cold Spring Harb Perspect Biol* 4: a005736
- Vizcaino JA, Csordas A, del-Toro N, Dianas JA, Griss J, Lavidas I, Mayer G, Perez-Riverol Y, Reisinger F, Ternent T, Xu QW, Wang R, Hermjakob H (2016) 2016 update of the PRIDE database and its related tools. *Nucleic Acids Res* 44: D447–D456
- Wanet A, Tacheny A, Arnould T, Renard P (2012) miR-212/132 expression and functions: within and beyond the neuronal compartment. *Nucleic Acids Res* 40: 4742–4753
- Wang ET, Cody NA, Jog S, Biancoletta M, Wang TT, Treacy DJ, Luo S, Schroth GP, Housman DE, Reddy S, Lecuyer E, Burge CB (2012) Transcriptome-wide regulation of pre-mRNA splicing and mRNA localization by muscleblind proteins. *Cell* 150: 710–724
- Yoshihara S, Takahashi H, Nishimura N, Kinoshita M, Asahina R, Kitsuki M, Tatsumi K, Furukawa-Hibi Y, Hirai H, Nagai T, Yamada K, Tsuboi A (2014) Npas4 regulates Mdm2 and thus Dcx in experience-dependent dendritic spine development of newborn olfactory bulb interneurons. *Cell Rep* 8: 843–857